Earth Science Informatics (2025) 18:466
https://doi.org/10.1007/s12145-025-01954-2

RESEARCH

Impact of major tropical volcanic eruptions on air temperatures in the Middle East

Gholamreza Roshan[1] · Abdolazim Ghanghermeh[1] · Stefan W. Grab[2] · Ecmel Erlat[3] · Murat Türkeş[4]

Received: 20 January 2025 / Accepted: 17 June 2025

Abstract

Although there has been extensive scientific work on the impacts of major volcanic eruptions on global and regional climates, the Middle East remains a knowledge gap in this regard. Our aim is to establish surface air temperature responses across the Middle East and easternmost Mediterranean basin, following three major tropical volcanic eruptions: Krakatau (1883), Agung (1963) and Pinatubo (1991). This study utilizes available data from CMIP6 climate models to analyze climatic responses to these eruptions. The longest-lasting cool anomalies, persisting for six years, followed the Krakatau eruption. The most pronounced post-Krakatau cooling occurred in 1884, with a regionally averaged temperature departure of -0.74 °C, relative to a mean baseline temperature. In contrast, the Agung eruption caused a regionally averaged temperature departure of -0.59 °C in 1964, but its cooling effect was more temporally limited, lasting approximately 3½ years. Air temperatures over the Middle East were depressed for over a decade following the Pinatubo eruption, but this may have been due to additional unidentified climatic factors. This extended cool period was marked by the strongest regionally averaged post-volcanic temperature departure of -0.76 °C, recorded in 1992. Our findings highlight that the extent of such cooling varied across the Middle East, with the most pronounced cooling occurring at higher elevations and latitudes, while southern regions (especially the Arabian Peninsula) experienced more moderate cooling. This study underscores that a combination of factors, including regional climate dynamics, have likely played a significant role in determining the intensity and duration of cooling associated with major volcanic eruptions, in the Middle East.

Keywords Major volcanic eruptions · Earth system · CMIP6 · Cooling effects · Middle East

Introduction

Volcanic eruptions are recognized as significant drivers of global and regional climate variability over periods from years to decades, primarily due to the injection of sulfur dioxide (SO2) into the stratosphere, where it forms sulfate aerosols (Uslular et al. 2022; Suhadha and Harintaka 2024). Volcanic sulfate aerosols alter the Earth's radiative balance, including tropospheric cooling through reflecting and scattering incoming solar radiation by absorbing incoming near-infrared and outgoing longwave radiation. The modifications in Earth's radiative balance and atmospheric chemistry after major volcanic eruptions may affect climate conditions in different ways, depending on the geographical location of the volcano, eruption magnitude and chemistry, timing (season) of the eruption, and existing global climatic situation at the time (e.g. Self 2006; Schmidt and Black 2022). While tropical eruptions typically have widespread and long-lasting effects due to their equatorial location and high-altitude SO2 injection, high-latitude volcanic eruptions tend to have more localized and short-lived climate impacts (Schneider et al. 2009; Timmreck 2018). The large-scale atmospheric effects of volcanic eruptions usually occur with a significant delay of

Communicated by: Hassan Babaie

✉ Abdolazim Ghanghermeh
a.ghangherme@gu.ac.ir

1 Department of Geography, Golestan University, Shahid Beheshti, Gorgan, Iran

2 School of Geography, Archaeology and Environmental Studies, University of the Witwatersrand, Johannesburg, South Africa

3 Department of Geography, Ege University, Bornova, İzmir, Turkey

4 The Center for Climate Change and Policy Studies and The Department of Physics, Boğaziçi University, İstanbul, Turkey

Published online: 07 July 2025

several months to two years after the eruption begins, due to the altered atmospheric chemistry and thus the affected radiation balance.

Observational and modelling studies have shown that major tropical eruptions, such as Tambora (1815), Krakatau (1883) and Pinatubo (1991), induce a global cooling of the Earth's surface climate by altering the incoming solar radiation. The Northern Hemisphere (NH) has been the subject of extensive study in this regard, with well-documented cooling effects observed in regions such as North America, Europe, and Asia (e.g. Briffa et al. 1998; Fischer et al. 2007; Raible et al. 2016; Stoffel et al. 2015; Erlat and Türkeş 2019; Zhu et al. 2024). The response to volcanic forcing in the Southern Hemisphere (SH) may manifest as significant cooling in some areas while some regions show more muted temperature declines possibly due to oceanic moderating effects (Wilmes et al. 2012; Colose et al. 2015; Harvey et al. 2020; Harvey and Grab 2021, 2022).

The cooling effects after major volcanic eruptions are both spatially and temporally intricate due to the sulphate aerosol distribution and possible feedbacks of the climate system (Man et al. 2014; Neukom et al. 2014; Sigl et al. 2015). For example, after the Agung eruption, globally mean top of the-atmosphere radiation anomalies were observed mainly in the SH, and therefore surface temperature anomalies were larger in the tropics and the SH (Bilbao et al. 2024). Modeling studies have reported a causal relationship between major volcanic eruptions and the positive phase of the Arctic Oscillation/North Atlantic Oscillation (AO/NAO) winter index through enhancing the stratospheric meridional temperature gradient (Coupe and Robock 2021; Paik et al. 2023).

Volcanic eruptions are among the most powerful natural forcings of the Earth's climate system. Their ability to inject large quantities of aerosols and gases into the stratosphere can lead to substantial short- and medium-term alterations in atmospheric circulation, surface temperatures, precipitation regimes, and regional climate dynamics. These disruptions can have far-reaching consequences for agriculture, water resources, ecosystems, and the frequency and intensity of extreme climate events (Robock 2000; Timmreck 2012). While the global climatic effects of major volcanic eruptions have been extensively studied, regional-scale assessments, particularly for the Middle East and North Africa (MENA), remain relatively limited. This is a critical gap, as the MENA region is highly sensitive to climatic variability and already experiences considerable stress on its water and agricultural systems. A growing body of research has begun to explore the regional climate responses to volcanic activity in the MENA, often with a focus on teleconnection mechanisms such as the North Atlantic Oscillation (NAO) and the El Niño–Southern Oscillation (ENSO). For example, Dogar et al. (2017) found that volcanic-induced cooling in the MENA is amplified during positive NAO phases, particularly in winter. In summer, volcanic forcing contributes to a weakening and southward displacement of the Intertropical Convergence Zone (ITCZ), suppressing the Indian and West African monsoons and leading to regional drying. Osipov and Stenchikov (2017) demonstrated, using coupled ocean-atmosphere models validated against observations, that the 1991 Pinatubo eruption significantly impacted Middle Eastern climate and Red Sea circulation. Their findings suggest that the observed cooling in winter was primarily driven by volcanic-induced changes in atmospheric circulation patterns, rather than direct radiative effects of aerosols alone. In Türkiye, Erlat and Türkeş (2019) identified a clear and statistically significant decline in both maximum and minimum temperatures during the 36 months following the eruptions of Agung (1963), El Chichón (1982), and Pinatubo (1991), with the cooling signal being strongest during the winter season. Seasonal asymmetries were observed, with maximum temperatures showing slightly stronger responses in spring and summer.

Paleoclimatic reconstructions also point to persistent hydroclimatic anomalies following large tropical eruptions. For instance, eruptions with sulfur emissions exceeding ~8 Tg S between 1000 and 1850 CE triggered prolonged drying across tropical Africa and the Middle East, which has been attributed to a southward ITCZ shift and changes in Pacific and Atlantic SSTs (Tejedor et al. 2021). Similarly, winter cooling in the MENA following major eruptions was not solely driven by ENSO phases; rather, El Niño conditions may have partially mitigated the cooling induced by concurrent positive NAO phases (Dogar et al. 2025). Despite these important contributions, a comprehensive, multi-eruption, model-based assessment of volcanic impacts on Middle East climate, particularly using the latest CMIP6 simulations, has not yet been undertaken. Many previous studies focus on isolated events or lack ensemble modeling approaches necessary for robust regional assessments. This study seeks to address this gap by systematically evaluating surface air temperature responses over the Middle East to three major tropical volcanic eruptions: Krakatau (1883), Agung (1963), and Pinatubo (1991). Utilizing multi-model CMIP6 outputs, we aim to (1) characterize the magnitude and spatial patterns of temperature anomalies associated with each eruption, and (2) situate these regional findings within a broader global context by comparing them with volcanic climate responses in other parts of the world.

Data and methods

Volcanic eruptions

The Volcanic Explosivity Index (VEI), established by Newhall and Self (1982), is widely employed to classify the relative magnitude of volcanic eruptions. Major volcanic eruptions are classified as having a Volcanic Explosivity Index (VEI) of 4 or higher (Newhall and Self 1982). To test the impact of major tropical volcanic forcing on temperatures in the Middle East, we select three relatively recent climatically impactful eruptions; namely Krakatau (1883; VEI = 6), Agung (1963; VEI = 5) and Pinatubo (1991; VEI = 6) (Table 1). The largest and these (Krakatau; Indonesia) occurred between 20 May and 21 October 1883, peaking on 26 August. The Agung (Indonesia) eruption lasted from February 1963 until January 1964, and Pinatubo (Philippines) erupted between April and September 1991 (Schaller et al. 2009; Fujiwara et al. 2015; Boretti 2024).

Methods

The latest phase of the Coupled Model Intercomparison Project (CMIP6) provides an advanced framework for simulating both historical and projected climate variations associated with volcanic eruptions through capturing aerosol concentrations and their interactions with the atmosphere (Hua et al. 2019; Toohey et al. 2019; McBride et al. 2021; Rong et al. 2021). CMIP6 simulations offer significant improvements over previous model generations by incorporating a higher spatial resolution and more detailed representations of aerosol microphysics, thereby providing more accurate projections of volcanic impacts (Zanchettin et al. 2015; Gerber et al. 2016; Wen-Min and Meng 2019). These models are particularly valuable for studying regions such as the Middle East, where limited observational data and underrepresentation in global studies have made it difficult to quantify the effects of volcanic eruptions. We thus use the CMIP6 archive to analyze the likely temperature responses to the three eruptions in the Middle East based on available model data. Fifty-seven CMIP6 models have been individually utilized to simulate temperature responses to selected volcanic eruptions (Eyring et al. 2016; O'Neill et al. 2016; Li et al. 2021). Each eruption was modeled separately, and the temperature results from all the models evaluated for each volcanic event. Reliable temperature data were obtained from 17 models for Krakatau, 12 models for Agung, and 20 models for Pinatubo (Table 2).

For each volcanic eruption, different CMIP6 models were selected based on their ability to reproduce the observed temperature changes associated with that specific eruption. This selection was made through the evaluation of model performance in capturing the observed temperature anomalies. Initially, for each model separately, temperature anomalies were calculated using a 12-month running mean over a 20-year period (5 years prior to and 15 years after the eruption) to separate the eruptions' effects from natural climate variability (Harvey et al. 2020; Harvey and Grab 2021). Statistical significance of these temperature anomalies for each model was assessed using the bootstrap resampling method with 5000 iterations. Additionally, the 5th and 95th percentiles for each model were calculated based on the 5-year period preceding the eruption. Models whose temperature changes during the eruption period exceeded these percentiles were considered as having simulated statistically significant temperature variations.

After selecting the best-performing models, the same statistical methodology was applied to the multimodel mean. To achieve this, model outputs were resampled at a 1° × 1° resolution and averaged to generate a multimodel mean for each eruption. Temperature anomalies for each multimodel mean were calculated using monthly air temperatures over a 5-year baseline period (i.e., 60 months) prior to each volcanic eruption. This baseline period served as the reference for determining anomalies (Rao et al. 2019).

To assess the statistical significance of the observed temperature changes in the multimodel mean, the same bootstrap method with 5000 iterations, which was applied to individual models, was used again. To test the robustness of the multimodel mean, the 25th and 75th percentiles of individual model responses to historical forcing experiments were considered. This step was particularly useful for distinguishing between random fluctuations and significant climatic responses. Additionally, the 5th and 95th percentiles were used to further distinguish between random variability and significant climatic changes based on established

Table 1 Selected major tropical (20 ºN – 20 ºS) volcanic eruptions and their locations, eruption date, volcanic explosivity index (VEI) and radiative forcing (data from Self and King, 1996; Shindell et al. 2004; Fischer et al. 2007; Myhre et al. 2013)

Volcano	Location		Date of major eruption	VEI	Emission (Tg SO2)	Radiative Forcing (W/m^2)
	Latitude	Longitude				
Mt. Krakatau (Indonesia)	6.1 °S	105.4 °E	26 August 1883	6.4	19	−3.6 W m^{-2}
Mt. Agung (Indonesia)	8.3 °S	115.5 °E	17 March 1963	5	11	-0.64/-1.19
Mt. Pinatubo (Philippines)	15.1 °N	120.4 °E	15 June 1991	6.1	18	-1.60/-3.73

Table 2 Selected climate models and datasets used to evaluate volcanic forcing (after Eyring et al. 2016; o'neill et al. 2016; Li et al. 2021)

Pinatubo	Krakatau	Agung
ACCESS-CM2 (Australia)	ACCESS-ESM1-5 (Australia)	ACCESS-CM2 (Australia)
BCC-CSM2-MR (China)	CanESM5-CanOE (Canada)	CIESM (China)
BCC-ESM1 (China)	CESM2-WACCM (USA)	CMCC-CM2-HR4 (Italy)
CanESM5 (Canada)	CIESM (China)	CNRM-ESM2-1 (France)
CIESM (China)	CMCC-ESM2 (Italy)	EC-Earth3-AerChem (Europe)
CMCC-CM2-HR4 (Italy)	CNRM-ESM2-1 (France)	FGOALS-f3-L (China)
CMCC-CM2-SR5 (Italy)	EC-Earth3-AerChem (Europe)	GFDL-ESM4 (USA)
E3SM-1-1-ECA (USA)	EC-Earth3-CC (Europe)	HadGEM3-GC31-LL (UK)
EC-Earth3-AerChem (Europe)	FGOALS-f3-L (China)	INM-CM4-8 (Russia)
FGOALS-g3 (China)	FIO-ESM-2-0 (China)	IPSL-CM6A-LR (France)
FIO-ESM-2-0 (China)	HadGEM3-GC31-LL (UK)	MIROC-ES2H (Japan)
INM-CM4-8 (Russia)	INM-CM4-8 (Russia)	NorESM2-MM (Norway)
IPSL-CM6A-LR (France)	INM-CM5-0 (Russia)	
KIOST-ESM (South Korea)	MCM-UA-1-0 (USA)	
MIROC6 (Japan)	MPI-ESM-1-2-HAM (Switzerland)	
MIROC-ES2L (Japan)	NESM3 (China)	
MPI-ESM1-2-HR (Germany)	NorESM2-MM (Norway)	
MPI-ESM1-2-LR (Germany)		
NorCPM1 (Norway)		
TaiESM1		

methodologies (e.g., Haurwitz and Brier 1981; Rao et al. 2017). These steps effectively minimized the influence of natural variability and ensured that the results were stable and statistically robust.

Validation of selected CMIP6 models using ECMWF reanalysis data

After selecting the top-performing CMIP6 models for each of the three volcanic eruptions under investigation (Agung, Pinatubo, and Krakatau), based on their ability to reproduce the observed temperature anomalies, the next step was to assess the accuracy of these selected models in replicating the climatic reality through comparison with reanalysis data. The goal of this stage was to determine whether the selected models, in addition to performing well in identifying significant temperature anomalies following the eruptions, also demonstrated sufficient validity when compared to independent reanalysis data.

Since reanalysis data for the periods corresponding to the Agung (1963) and Pinatubo (1991) eruptions are available from the ECMWF database, the validation process was only feasible for these two events. For this purpose, temperature time series for the Middle East region were first extracted from the ECMWF database. Subsequently, the temperature outputs from the selected models for these two eruptions were statistically compared with the ECMWF data.

To perform this comparison, the "Random Forest" machine learning algorithm, known for its precision in classification and regression, was utilized. This algorithm constructs a set of decision trees, and through GridSearchCV and 5-fold cross-validation, the key model parameters, including the number of trees (n_estimators), tree depth (max_depth), and the minimum number of samples required for node splitting (min_samples_split), were optimized (Collins et al. 2006).

For quantitative performance evaluation, the statistical indices of R^2 (Coefficient of Determination), RMSE (Root Mean Square Error), and NSE (Nash–Sutcliffe Efficiency) were calculated to assess the model's ability to explain data variance, measure prediction accuracy, and evaluate the model's performance relative to the mean of observational data. Models that demonstrated strong statistical performance in this evaluation not only succeeded in identifying temperature anomalies associated with the eruptions but were also deemed reliable when compared to independent reanalysis data. The results of this stage thus provide further confirmation of the selection of the best models, serving as a strong foundation for the final analysis in this study.

Study region

The Middle East spans a wide and diverse geographic region between latitudes 12°N and 42°N and longitudes 25°E and 60°E (Fig. 1). The region is bounded by the Mediterranean Sea to the west, the Indian Ocean to the south, and the mountainous ranges of Iran and Turkey to the north, giving rise to a variety of climatic and geographical features (Issar 2003; Issar & Zohar 2007). This region is predominantly characterized by dry summer subtropical Mediterranean and semi-arid steppe climates. Arid and hyper-arid desert climatic conditions occur over much of the Arabian Peninsula, Syria, Iraq, and Iran (Türkeş 2017). Annual rainfall is generally low (<250 mm), though mountainous and coastal areas benefit from higher precipitation (Tramblay et

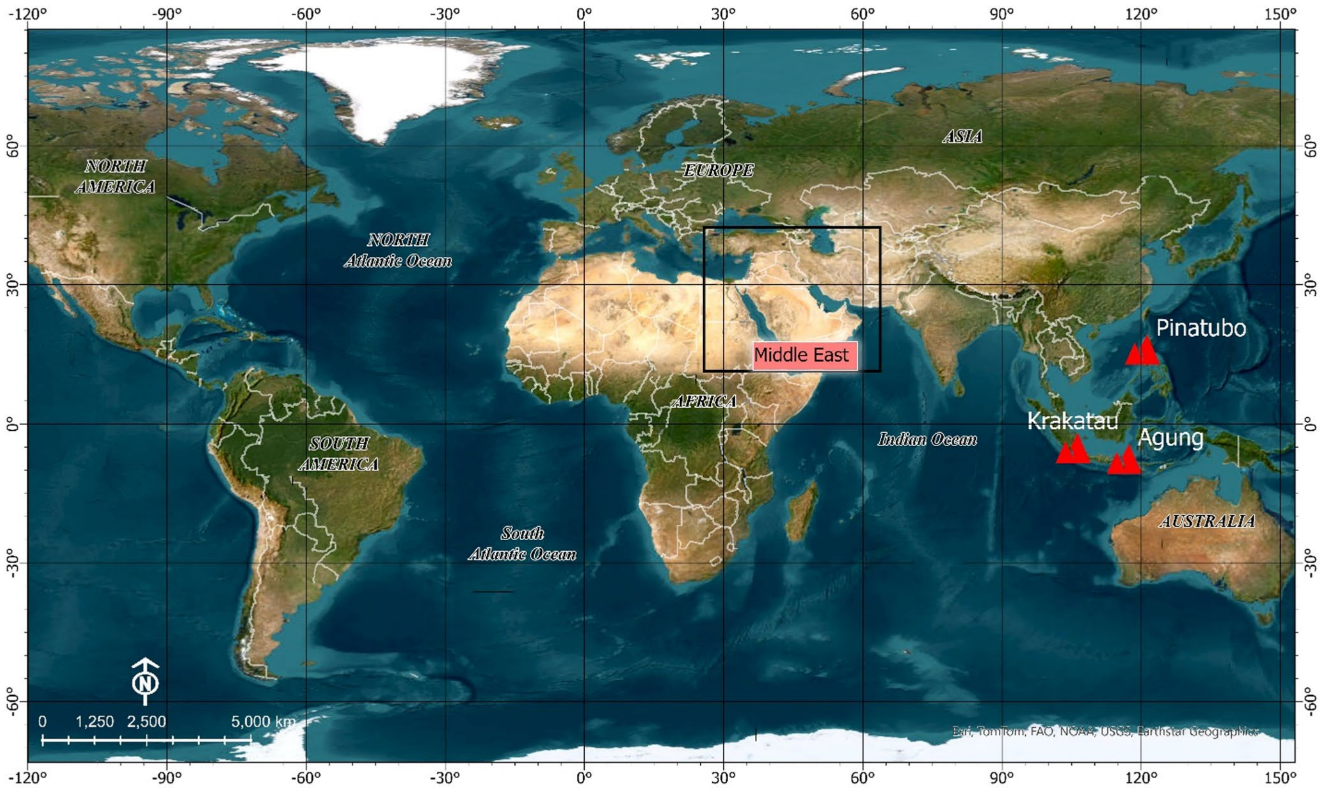

Fig. 1 Geographical location of the study region and the three volcanoes considered for this study

Table 3 Validation of selected climate models using ECMWF data for the Agung eruption during the 1958–1978 period

Selected models	R^2	RMSE	NSE
ACCESS-CM2	0.876	0.125	0.876
CIESM	0.862	0.091	0.862
CMCC-CM2-HR4	0.848	0.097	0.848
CMCC-ESM2	0.865	0.116	0.865
EC-Earth3-AerChem	0.883	0.106	0.883
FGOALS-f3-L	0.834	0.132	0.834
GFDL-ESM4	0.849	0.104	0.849
HadGEM3-GC31-LL	0.860	0.113	0.860
INM-CM4-8	0.835	0.113	0.835
IPSL-CM6A-LR	0.857	0.089	0.857
MIROC-ES2L	0.860	0.123	0.860
NorESM2-MM	0.841	0.143	0.841
The multimodel mean	0.850	0.063	0.850

al. 2020; Turkes et al. 2020; Zittis et al. 2022; Neira et al. 2023). Mediterranean areas of the region, such as western and southern Turkey, Lebanon, western and northern Syria, northern Iraq, north-northwest Iran and Israel, experience dry summers and cool, wet winters (Issar and Zohar 2007; Turkes, 2020; Türkeş 2022). However, there is substantial climatic variability; regions such as Iran and Turkey experience cold continental-type winters with snowfall at higher elevations and latitudes.

Results

Evaluation of climate model performance using reanalysis data

The validation results of the selected climate models, compared to ECMWF data over a five-year period before, and fifteen years after the Agung volcanic eruption, are presented. This evaluation is based on statistical metrics including the coefficient of determination (R^2), root mean square error (RMSE), and Nash-Sutcliffe efficiency (NSE) (Table 3). The R^2 values for all models range from 0.834 to 0.885, reflecting their strong ability to explain the variance in the observational data. Although all models perform within acceptable limits, the EC-Earth3-AerChem model, with R^2 and NSE both equal to 0.883 and RMSE = 0.106, exhibits the best performance. In contrast, the FGOALS-f3-L model, with R^2 = 0.834, NSE = 0.834, and RMSE = 0.132, demonstrates relatively weaker performance, although its results remain within an acceptable range. Models such as ACCESS-CM2 and CIESM, with R^2 values of 0.876 and 0.862, and NSE values of 0.876 and 0.862, respectively, show better performance compared to the other models. Additionally, the ensemble mean of the selected models, with R^2 = 0.885, NSE = 0.885, and RMSE = 0.063, demonstrates a particularly strong correlation with ECMWF data.

These results provide robust evidence for the high reliability of the selected models in simulating the temperature responses to the Agung eruption.

Table 4 presents the validation results of the selected climate models, compared to ECMWF data over the five years preceding, and fifteen years following the eruption of Pinatubo. The results indicate that the R^2 values for all models range from 0.928 to 0.989, showcasing their strong ability to explain the variance in ECMWF observational data. As shown, all models perform well, with the multimodel mean providing the best performance, exhibiting R^2 and NSE values of 0.989 and the lowest RMSE of 0.031, reflecting excellent agreement with ECMWF data. In contrast, the KIOST-ESM model, with R^2 = 0.928, NSE = 0.928, and the highest RMSE of 0.109, demonstrates relatively weaker performance compared to the other models, although its results are still within an acceptable range. Models such as BCC-CSM2-MR, with R^2 and NSE values of 0.943 and RMSE = 0.085, and CanESM5, with R^2 and NSE values of 0.982 and RMSE = 0.054, exhibit very strong performance, yielding results comparable to the best-performing models. Overall, these findings highlight the high reliability of the selected models in simulating ECMWF data during the period associated with the Pinatubo eruption. This further supports the validity of these models in simulating climatic responses to major volcanic events.

Table 4 Validation of selected climate models using ECMWF data for the Pinatubo eruption during the 1987–2006 period

Selected models	R^2	RMSE	NSE
ACCESS-CM2	0.941	0.090	0.941
BCC-CSM2-MR	0.943	0.085	0.943
BCC-ESM1	0.951	0.083	0.951
CIESM	0.962	0.059	0.962
CMCC-CM2-HR4	0.958	0.072	0.958
CMCC-CM2-SR5	0.918	0.100	0.918
CanESM5	0.982	0.054	0.982
E3SM-1-1	0.968	0.077	0.968
EC-Earth3-AerChem	0.976	0.086	0.976
FGOALS-g3	0.958	0.079	0.958
INM-CM4-8	0.975	0.057	0.975
IPSL-CM6A-LR	0.940	0.072	0.940
KIOST-ESM	0.928	0.109	0.928
MIROC-ES2L	0.947	0.086	0.947
MIROC6	0.956	0.083	0.956
MPI-ESM1-2-HR	0.927	0.090	0.927
MPI-ESM1-2-LR	0.950	0.067	0.950
NorCPM1	0.948	0.073	0.948
TaiESM1	0.978	0.065	0.978
The multimodel mean	0.989	0.031	0.989

Air temperatures in the Middle East following the Krakatau (1883) eruption

To establish Krakatau's impact on temperature in the Middle East, a mean baseline temperature was calculated for the period from 1878 to 1882, and subsequent temperature variability measured relative to this baseline average. Only those temporal temperature variations that indicate statistically significant increases or decreases are discussed. It is often observed that a cooling pattern precedes volcanic eruptions. As explained in the Materials and Methods section, the analysis incorporates a moving average filter applied to the dataset to smooth short-term fluctuations and emphasize long-term trends. This smoothing method inherently blends pre-eruption and post-eruption data, which can introduce an apparent cooling signal leading up to the eruption dates. This effect is a known limitation of using moving averages in time-series analysis, as the filter attributes a portion of the post-eruption cooling trend to the pre-eruption period. Other studies employing similar smoothing techniques have also reported analogous artifacts. For instance, Robock (2000) highlights how data preprocessing methods can sometimes obscure the exact temporal boundaries of volcanic impacts on climate. Thus, the observed pre-eruption cooling is not a direct climatic response but rather a methodological artifact of the moving average approach.

The cooling trend observed before the Krakatau eruption corresponds to one of the years in which the highest positive anomalies (+3.01) was observed in the 1881-82 NAO winter index (CRU, 2024). Krakatau had a large-scale cooling effect and left notable temperature anomalies in Middle East. Temperature departures from the 1878–1882 baseline for the time series between 1878 and 1898 indicate a cooling trend in the Middle East lasting 75 months, from July 1883 to September 1889 (Fig. 2). During this period, the regionally averaged temperature departure was −0.34 °C, with the most pronounced negative departures recorded in June and May 1884 (-0.74 °C and −0.73 °C, respectively). The volcanic eruption had a direct cooling effect on temperature, which was most pronounced during the first 12 months following the eruption, until June 1884. After this period, the cooling effect dissipated. However, despite the increase in temperature after June 1884, it took nearly 63 months for temperatures to return to pre-eruption conditions. The major (VEI 5) Tarawera (38°13'S; 176°31'E) eruption in June 1886 may have provided additional cooling and slowed the temperature recovery associated with Krakatau (see Rampino and Self 1982; Picas and Grab 2020).

Following October 1889, a phase of positive temperature departures is observed for 11 months, signaling the end of Krakatau's cooling influence on Middle Eastern temperatures. However, after this warming period, a new cooling

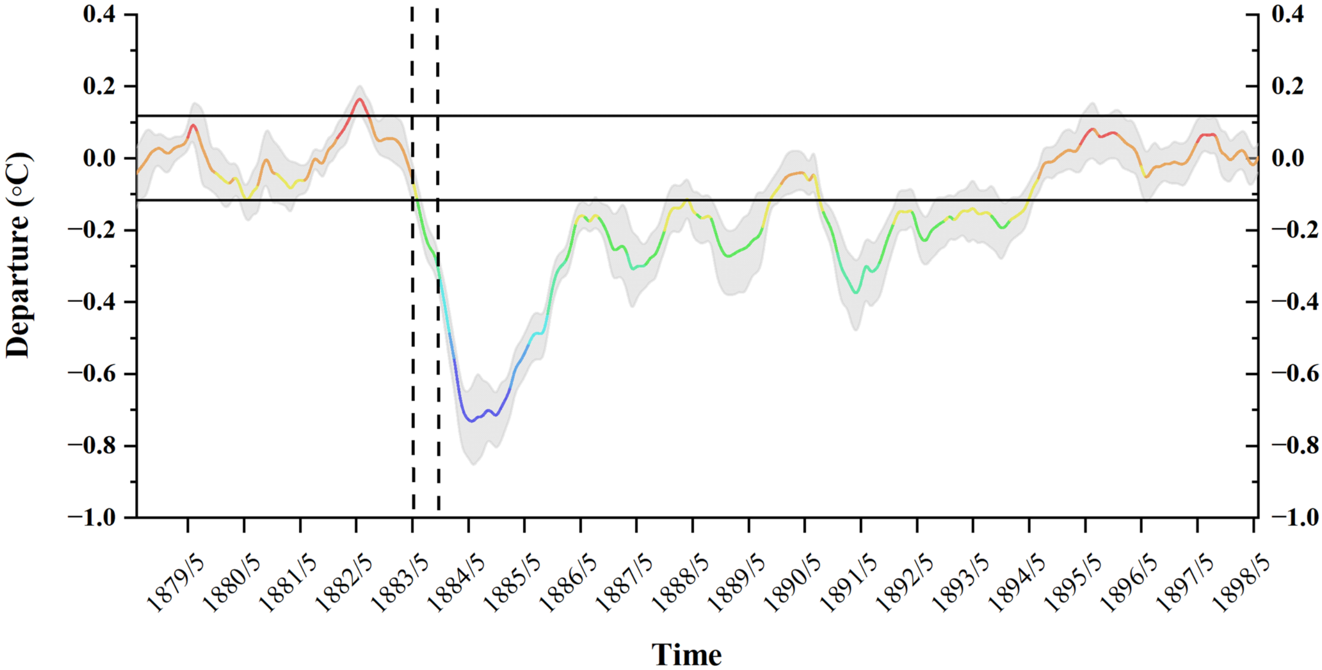

Fig. 2 CMIP6- Derived 12-month moving average of temperature anomalies for the Middle East: 1879–1898. Vertical dashed lines mark the eruption phase of Krakatau, from May to October 1883. Solid lines indicate the 90% confidence level, and grey shading represents the ensemble spread (25th to 75th percentiles)

trend emerged in September 1890 and persisted for 44 months until April 1894, with an average negative temperature departure of -0.21 °C. Given the preceding warming phase from October 1889 to August 1890, which showed no statistically significant changes, it is unlikely that the subsequent cooling phase was directly attributable to the Krakatau eruption. Overall, early indications of a return to pre-eruption baseline temperature conditions are evident during the first half of 1890 (Fig. 2).

The strongest negative temperature departure (-0.8 °C) in 1884 affected approximately 24.86% of the area (Fig. 3). The cool anomaly persisted until 1887, impacting 77.28% of the Middle East. In the first post-eruption year, cooling had spread across 99.97% of the Middle East, with nearly half of the region (46.75%) recording temperature departures between −0.6 °C to -0.8 °C. In the second post-eruption year, almost the entire region (99.69%) remained within the range of -0.01 °C to -0.8 °C from baseline conditions, and 60.37% of the region continued experiencing significantly cool conditions (departures of -0.6 °C to -0.8 °C).

Figure 4 displays maps that illustrate both annual and seasonal temperature departures from that of the baseline mean. These maps depict temperature departures for the eruption year and the subsequent four years, providing a detailed spatial-temporal analysis of temperature fluctuations across the study region. Figure 4 illustrates a consistent cooling trend across the entire study region during the eruption year, with negative temperature departures primarily ranging from −0.01 °C to -0.19 °C. Notably, a band extending from central to eastern Iran displays a contrasting positive temperature departure of up to +0.2 °C. In winter, most of the Middle East, apart from western regions, experienced positive temperature departures ranging from 0 °C to 0.2 °C, with a core area in southwestern Iran indicating departures of between 0.21 °C and 0.4 °C. During spring, negative temperature departures were observed across most regions, except for the central and northeastern Middle East, which experienced departures of up to +0.2 °C. As summer transitioned into autumn, the northern Middle East recorded strongest temperature reductions, with departures ranging from −0.41 °C to -0.59 °C. The most significant negative temperature departure occurred in 1884, though substantial cooling persisted into 1885. By 1886/7, considerable temperature recovery is noted, with southeastern regions of the Middle East (including the Arabian Peninsula and southeastern Iran) indicating positive temperature departures (Fig. 4).

Air temperatures in the Middle East following the Agung (1963) eruption

As depicted in Fig. 5, a clear and prolonged negative temperature anomaly is evident from May 1963 to November 1969, lasting 43 months. It is worth noting that prior to the occurrence of the studied volcanic eruption, a strong negative phase of the North Atlantic Oscillation (NAO), with an intensity of -2.47, was experienced in March and July 1962.

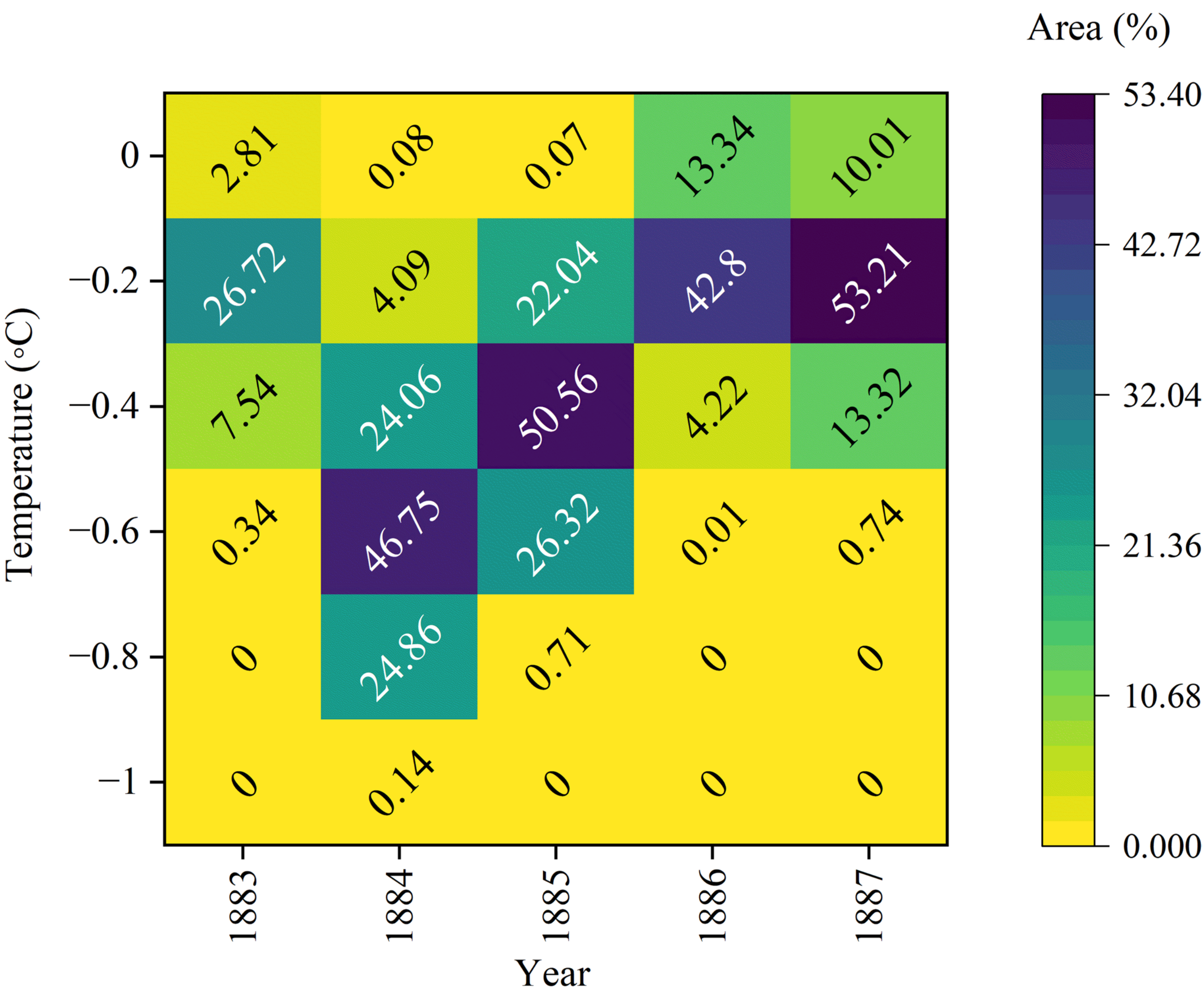

Fig. 3 The spatial extent (%) of statistically significant negative temperature departures in the Middle East during and after the Krakatau eruption

This phase may have contributed to cooling of the region before the eruption. The average temperature departure during this period was −0.43 °C, with the most pronounced decline occurring in May 1964 (-0.59 °C). While a significant negative temperature departure is observed across the entire 43-month period, several fluctuations are noted. A strong temperature reduction is recorded from May 1963 (-0.29 °C) to May 1964 (-0.59 °C). This is followed by a warming trend from June 1964 (-0.58 °C) to January 1965 (-0.38 °C). Cooling again occurs between February 1965 (-0.39 °C) and October 1965 (-0.49 °C), followed by warming from November 1965 (-0.48 °C) to November 1966 (-0.27 °C). Two additional cooling phases were observed: one from September 1967 to November 1968 (mean departure of -0.35 °C), and another from September 1970 to September 1971 (mean departure of -0.34 °C).

Nevertheless, several volcanic events with VEI values below 3, including those at Mount Etna (Italy) and Cerro Hudson (Chile) between 1969 and 1971, may have had a relatively limited yet notable influence on the negative temperature anomaly observed during this period. However, the results indicate that following November 1966, a period of limited temperature variability occurred for nine months (December 1966 to August 1967), which implies that the cooling observed after August 1967 cannot be directly attributed to the Agung eruption. Additionally, from September 1972 to June 1978, temperatures gradually increased, eventually reaching mean baseline values (1958–1962) in 1976 (Fig. 5).

Significant and negative temperature departures were observed up to 3½ years after the eruption. During the eruption year (1963), 36.58% of the study area experienced negative temperature departures ranging from −0.01 °C to

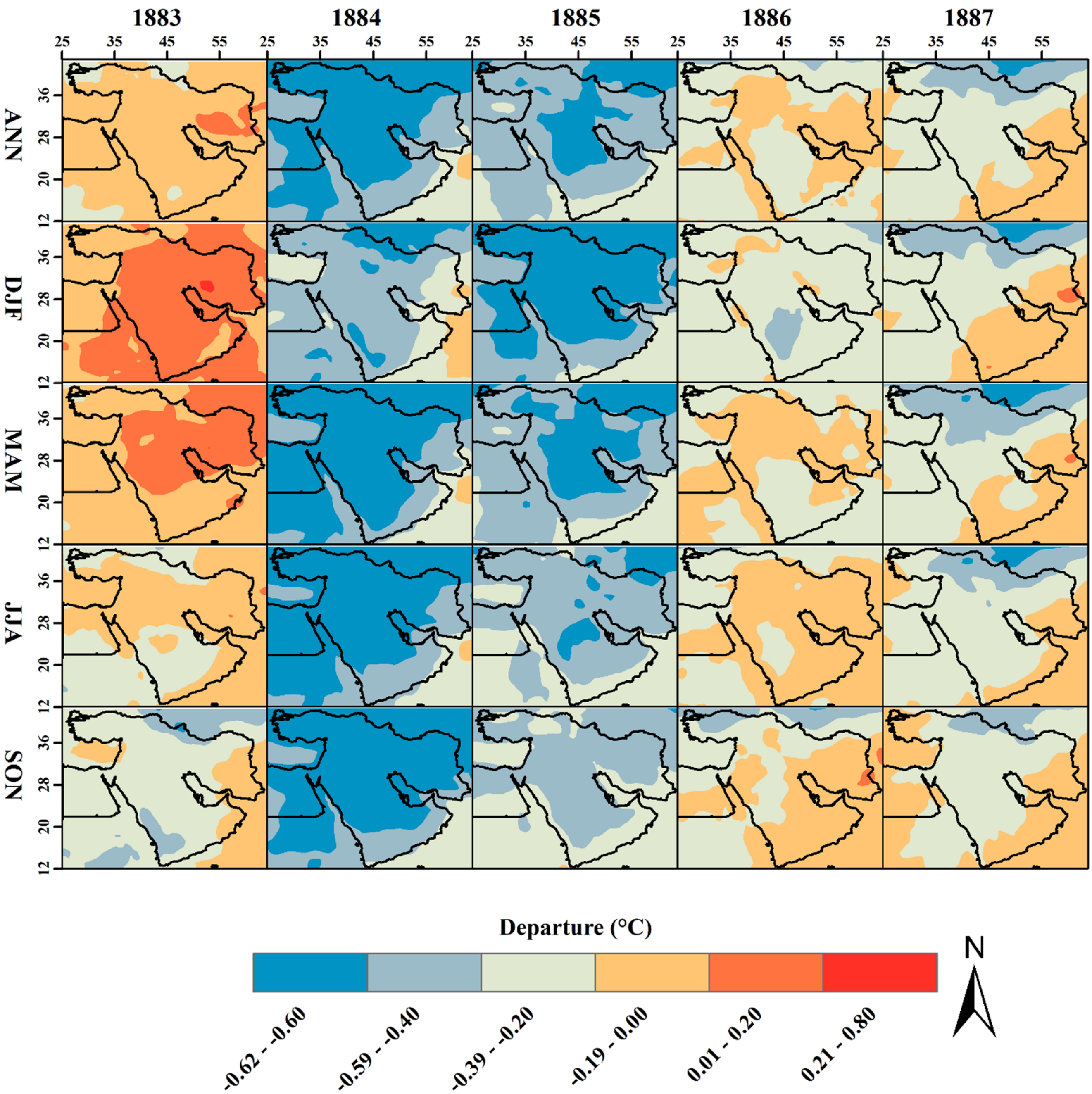

Fig. 4 Annual and seasonal temperature departures (1883–1887) relative to the five-year baseline before the Krakatau eruption, where only cooling in the range of -0.20 to -0.62 °C is statistically significant

-0.8 °C (Fig. 6). As much as 19.23% of the region experienced temperature departures of -0.4 °C to -0.6 °C. During the post-eruption year (1964), cool anomalies (-0.2 °C to -1 °C) had spread to over 93.95% of the Middle East. The maximum negative temperature departure associated with Agung reached −1.0 °C but affected only 1.04% of the region (the northwestern borders of Iran and the eastern border strip of Turkey). During the second post-eruption year (1965), 85.5% of the study area still experienced temperature departures ranging from −0.2 °C to -0.8 °C, however, the areas impacted by such departures declined to 63.27% in 1966 and 29.78% in 1967 (Fig. 6).

Figure 7 presents the annual and seasonal temperature anomalies (departures) relative to the baseline period of 1958–1962, visualized in map form. The figure demonstrates a distinct negative temperature departure across the entire region during the year of the volcanic eruption. For both annual and seasonal periods, the lowest negative

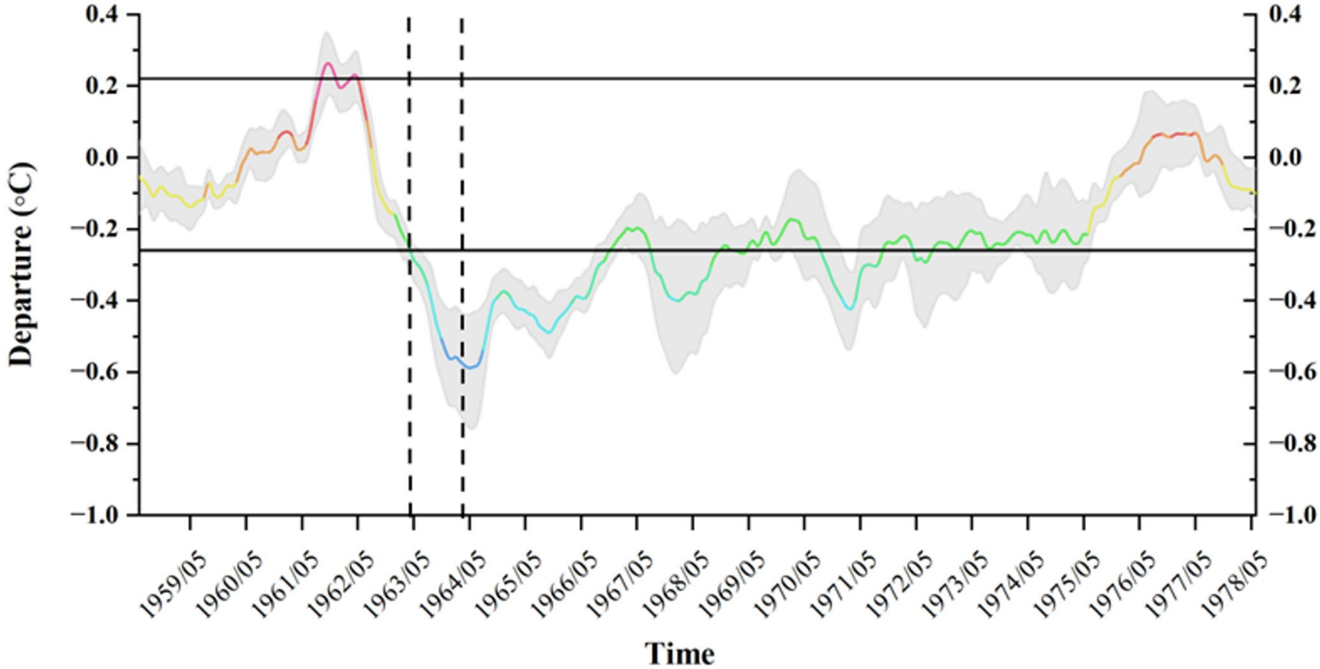

Fig. 5 CMIP6-Derived 12-month moving average of temperature anomalies for the Middle East: 1958–1979. Vertical dashed lines mark the eruption phase of Agung, from February 1963 to January 1964. Solid lines indicate the 90% confidence level, and grey shading represents the ensemble spread (25th to 75th percentiles)

temperature departures (ranging from −0.01 °C to -0.19 °C) are measured in the southeastern portion of the region, primarily covering areas of Saudi Arabia, Oman, Yemen, and parts of Iran. These areas, which are predominantly dry and desert regions, exhibit the most minimal temperature changes during the study period.

Seasonally, the most pronounced negative temperature anomalies are observed during the winter months, where a large portion of the region experienced departures ranging from −0.01 °C to -0.19 °C. Conversely, certain areas in the northeast and south display positive temperature anomalies, with departures reaching up to +0.2 °C. As shown in Fig. 7, the most significant negative temperature anomalies (exceeding −0.6 °C) occurred in autumn, coinciding with the eruption year; this cooling subsequently intensified, surpassing that of other seasons. In the first year following the eruption, a widespread negative temperature anomaly is observed across the entire study area, with the cooling intensity being stronger than in subsequent years (Fig. 7).

It is important to emphasize that the northern half of the region, which includes the elevated and mountainous plateaus of western Asia (such as the mountainous areas of Iran, Turkey, northern Iraq and Syria), experienced more substantial negative temperature anomalies than the southern half, encompassing the Arabian Peninsula and the arid regions of southwest Asia. While autumn exhibited the strongest cooling during the eruption year, this was not the case during the year following the eruption, when autumn cooling anomalies were lower than for other seasons. This is likely due to the timing of the Agung eruption in autumn 1963 having directly contributed to the heightened negative temperature anomalies observed during that season. By 1965, the maximum cooling intensity shifted to northeastern areas, and by 1966 and 1967, the extent of areas experiencing severe cooling (below −0.6 °C) had diminished. In 1967, shallower temperature departures of between 0 °C and −0.19 °C had become more widespread than in previous years (Fig. 7).

Air temperatures in the Middle East following the Pinatubo (1991) eruption

As shown in Fig. 8, from August 1991 onward, temperature departures following the Pinatubo eruption reached −0.14 °C. The average negative temperature anomaly during this 110-month period of 1991–2000 was −0.32 °C. The most pronounced negative temperature anomalies took place between August 1991 and July 1992, with an average departure of -0.49 °C and strongest departure of -0.76 °C in July 1992. From August 1992 to March 1996, rapid temperature recovery occurred, with an average departure of -0.39 °C. Thereafter, from April 1996 to September 2000, temperatures recovered more gradually (apart from a strong cool anomaly during 1998/9). The climatic consequences of the Pinatubo eruption in the Middle East indicate that by the

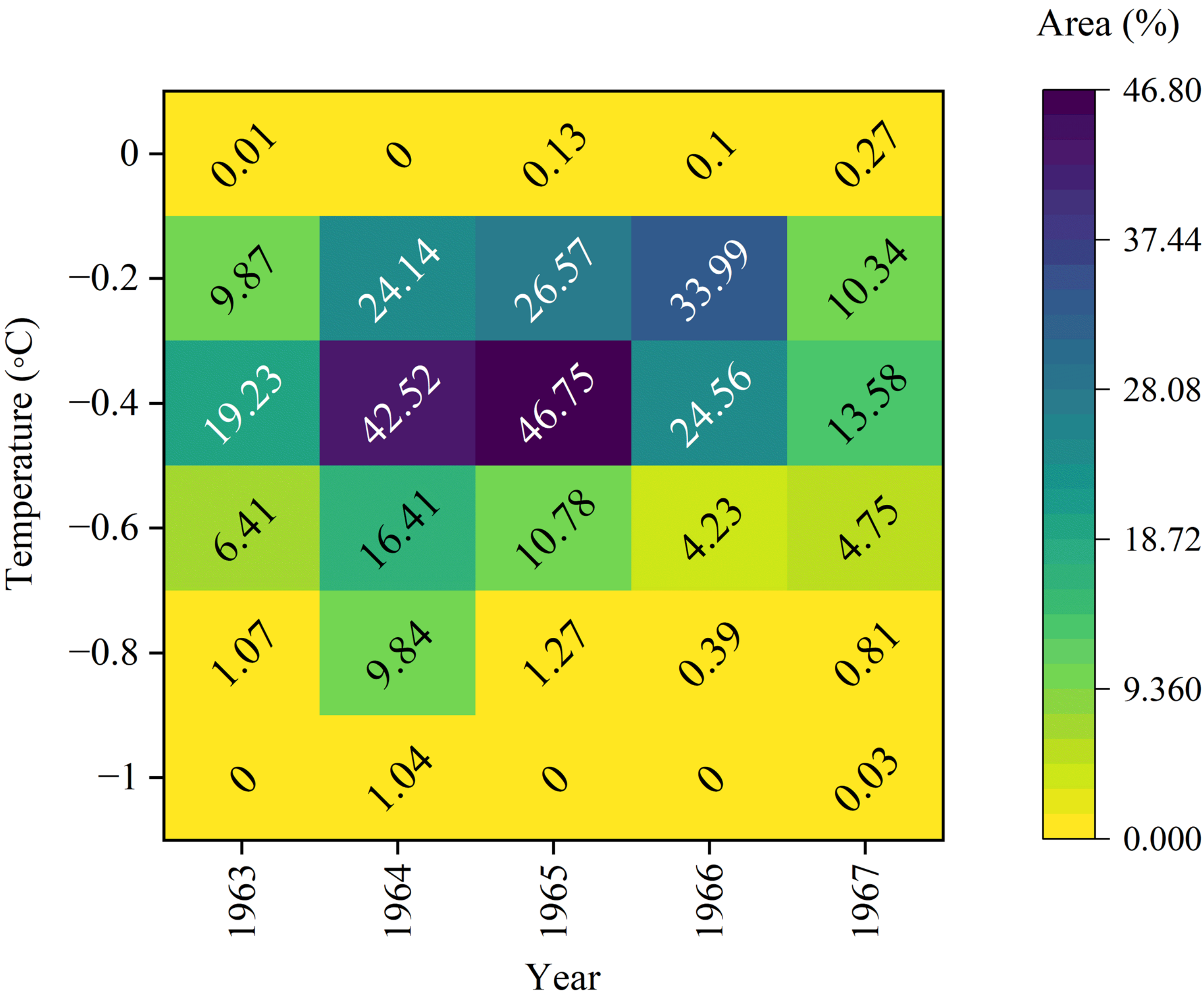

Fig. 6 The spatial extent (%) of statistically significant negative temperature departures in the Middle East during and after the Agung eruption

end of 2000 and the beginning of 2001, temperatures had returned to the 1986–1990 baseline conditions (Fig. 8).

During the eruption year, 34.85% of the study area experienced significant negative temperature departures of up to -0.8 °C (Fig. 9). The largest negative temperature departures, which occurred over 17.59% of the area, ranged from −0.2 °C to -0.4 °C. During the post-eruption year (1992), almost all of the Middle East (99.06% of the region) experienced negative temperature departures in the range −0.01 to -1 °C. Strong negative temperature anomalies (-0.6 °C to -0.8 °C) affected 44.27% of the region in 1992. However, the strongest departures of -1 °C, only affected a small portion (2.3%) of the region in 1992. During 1993, 99.39% of the Middle East continued to experience negative temperature departures of between −0.01 °C and −0.8 °C, with 47.27% of the region recording departures of between −0.4 °C and −0.6 °C. Cooling continued into 1994/5, affecting 92.29% and 94.66% of the region, respectively (Fig. 9).

During the Boreal autumn of the Pinatubo eruption year, a broad 'belt' of negative temperature anomalies (up to -0.19 °C) extending from the southwest to the northeast, had emerged (Fig. 10). However, in northern parts, as well as eastern Saudi Arabia and the Gulf of Oman, positive temperature anomalies (+0.2 °C) are observed. Strongest cooling is observed in autumn, especially over northwestern parts of the Middle East, including the Zagros Plateau and its surrounding regions (encompassing northwestern Iraq and the borders with Turkey and Syria). During the post-eruption year (1992), the entire Middle East experienced cooling. Apart from northwestern and southeastern regions, most of the Middle East recorded strong temperature departures of between −0.60 °C and −0.62 °C. Winter was the least affected season in 1992, particularly over northwestern

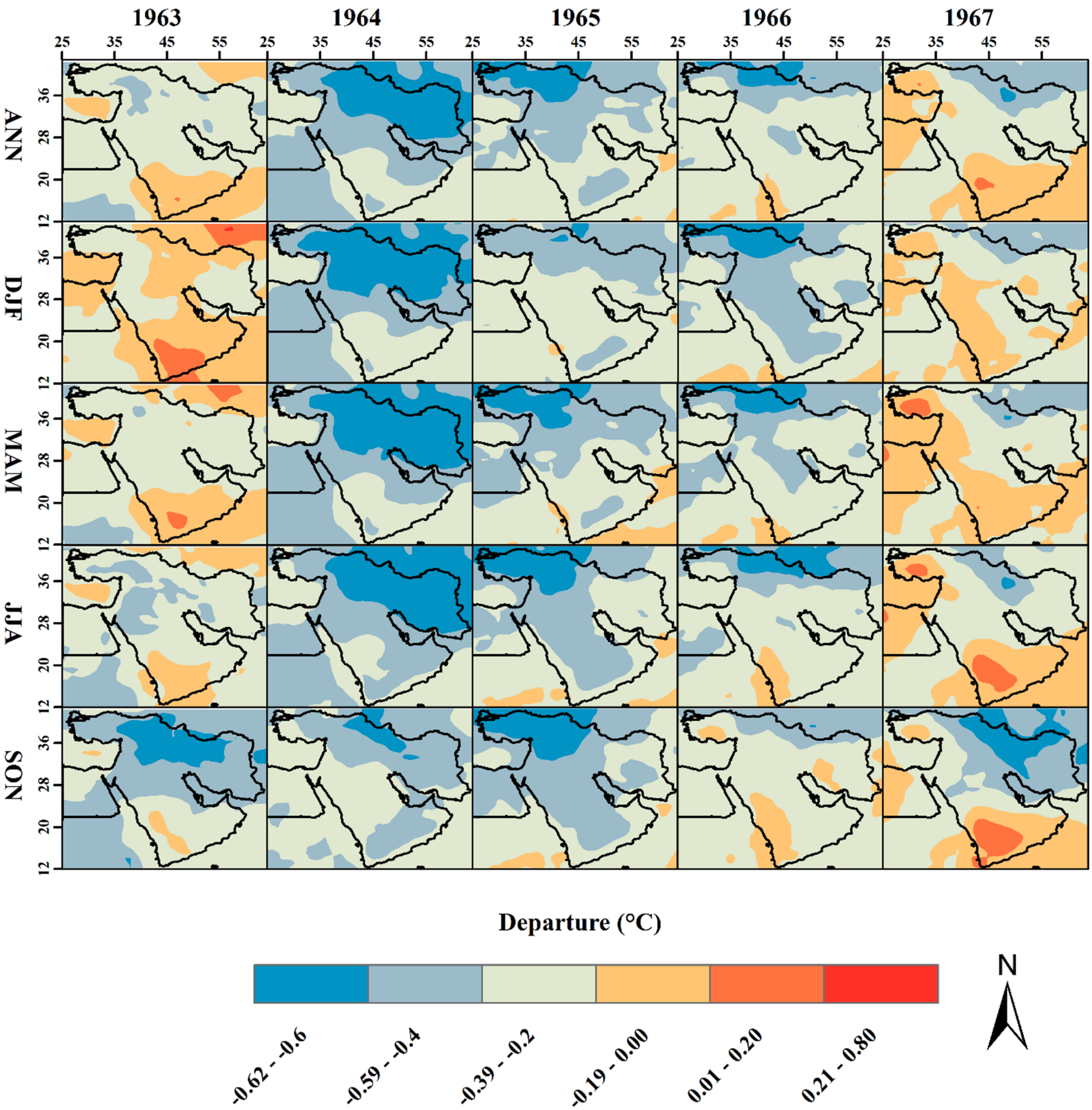

Fig. 7 Annual and seasonal temperature departures (1963–1967) relative to the five-year baseline before the Agung eruption, where only cooling in the range of -0.20 to -0.62 °C is statistically significant

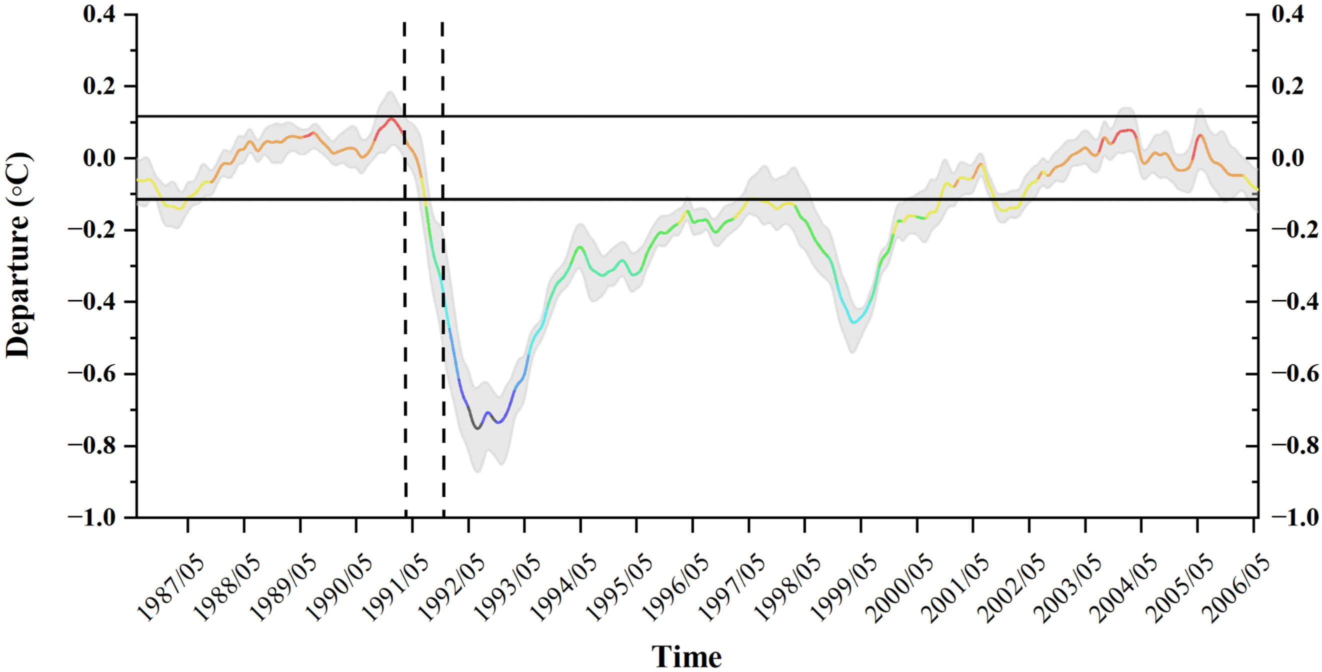

Fig. 8 CMIP6-Derived 12-month moving average of temperature anomalies for the Middle East: 1986–2007. Vertical dashed lines mark the eruption phase of Pinatubo, from April to September 1991. Solid lines indicate the 90% confidence level, and grey shading represents the ensemble spread (25th to 75th percentiles)

parts of the Middle East and west Asia (including the Zagros Plateau and the plains between the Tigris and Euphrates); here departures ranged between −0.01 °C and −0.19 °C. In contrast, during 1993, strongest seasonal cool anomalies occurred during winter, which was followed by a warming trend from spring onwards. Temperature recovery seemed most rapid in far northeastern parts, including parts of northeastern Turkey and Azerbaijan (part of the Caucasus) (Fig. 10). In 1994/5, temperatures returned to near-normal, with some localized warm anomalies in northern Iran, Turkey, and the Persian Gulf region.

Discussion

Uncertainties in CMIP6 models: climate sensitivity and aerosol forcing

Recent discussions regarding CMIP6 models have highlighted significant controversy regarding their assumed climate sensitivity. One of the main concerns is the substantial increase in equilibrium climate sensitivity (ECS) across several CMIP6 models compared to previous model generations, raising doubts about the reliability of future climate projections (Zelinka et al. 2020; Nijsse et al. 2020). This discrepancy is largely attributed to differences in cloud feedbacks and the representation of radiation processes, leading to a broader and more uncertain range of ECS estimates. However, CMIP6 models have shown improvements over previous generations (CMIP5) in certain areas. In particular, in simulating volcanic eruption impacts and oceanic temperature changes, CMIP6 models have demonstrated notable progress. They have shown improved performance in simulating surface temperature changes following eruptions such as the 1991 eruption of Pinatubo, with better predictions for regions such as the North Atlantic (Eyring et al. 2016; Rieger et al. 2020). Moreover, the role and strength of aerosol forcing, particularly sulfate aerosols, remain highly debated within the scientific community. Aerosols cool the climate by increasing Earth's albedo and modifying cloud properties. However, the strength of this cooling effect has undergone significant revisions in recent years, leading to increased uncertainty in the impact of aerosols on climate models (Smith et al. 2020). Some studies suggest that CMIP6 models represent a weaker aerosol cooling effect compared to previous generations, which could explain the higher ECS values and stronger warming projections in these models. Yet, other studies argue that aerosol forcing may still be strong, but due to updated emission inventories and improved aerosol-cloud interaction representations, it is modeled differently in CMIP6 (Meehl et al., 2014). These differing views on climate sensitivity and aerosol forcing highlight the importance of considering uncertainties in CMIP6 outputs when interpreting regional climate impacts. The ongoing debates within the scientific community play a crucial role in shaping our understanding of climate model

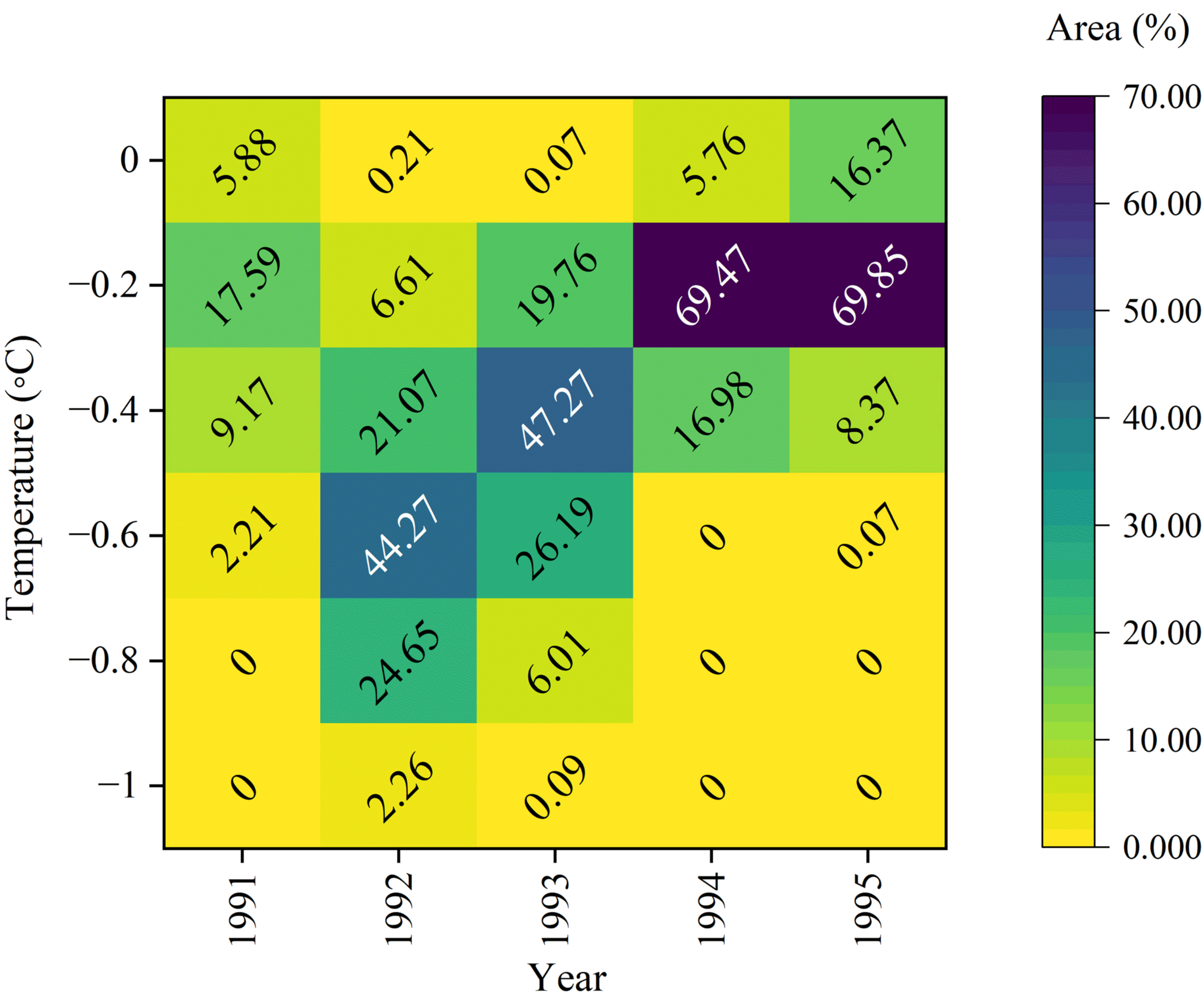

Fig. 9 The spatial extent (%) of statistically significant negative temperature departures in the Middle East during and after the Pinatubo eruption

projections, particularly for studies involving volcanic impacts, as the strength of aerosol forcing can directly influence temperature anomalies.

Temperature responses in a global context

Our aim in this discussion is to place Middle Eastern air temperature responses following the three major volcanic eruptions (Krakatau 1883, Agung 1963, and Pinatubo 1991) in a global context. While temperature departures can, in principle, represent both cooling and warming, in the context of this study we focus specifically on the cooling effects observed after major volcanic eruptions. The interpretation of such anomalies remains complex due to the influence of internal climate variability and short-term atmospheric fluctuations, such as ENSO and NAO, which can temporarily mask or amplify the volcanic signal (Thompson et al. 2009). To address this, we applied a 12-month running mean over the 20-year study period, along with the use of multi-model means, in order to reduce internal variability ('noise') and better isolate the volcanic response. Nevertheless, we acknowledge that residual uncertainties may still influence the attribution of volcanic cooling signals, particularly at regional scales. As such, temperature departures should be interpreted with caution and within the context of these methodological constraints.

Krakatau 1883

The August 1883 Krakatau eruption caused a mean NH temperature departure of -0.3 °C in 1884, followed by gradual warming, based on paleo-records (Zielinski 2000). However, earlier work by Self et al. (1981) and Rampino and Self (1982), based on observational station data, demonstrated

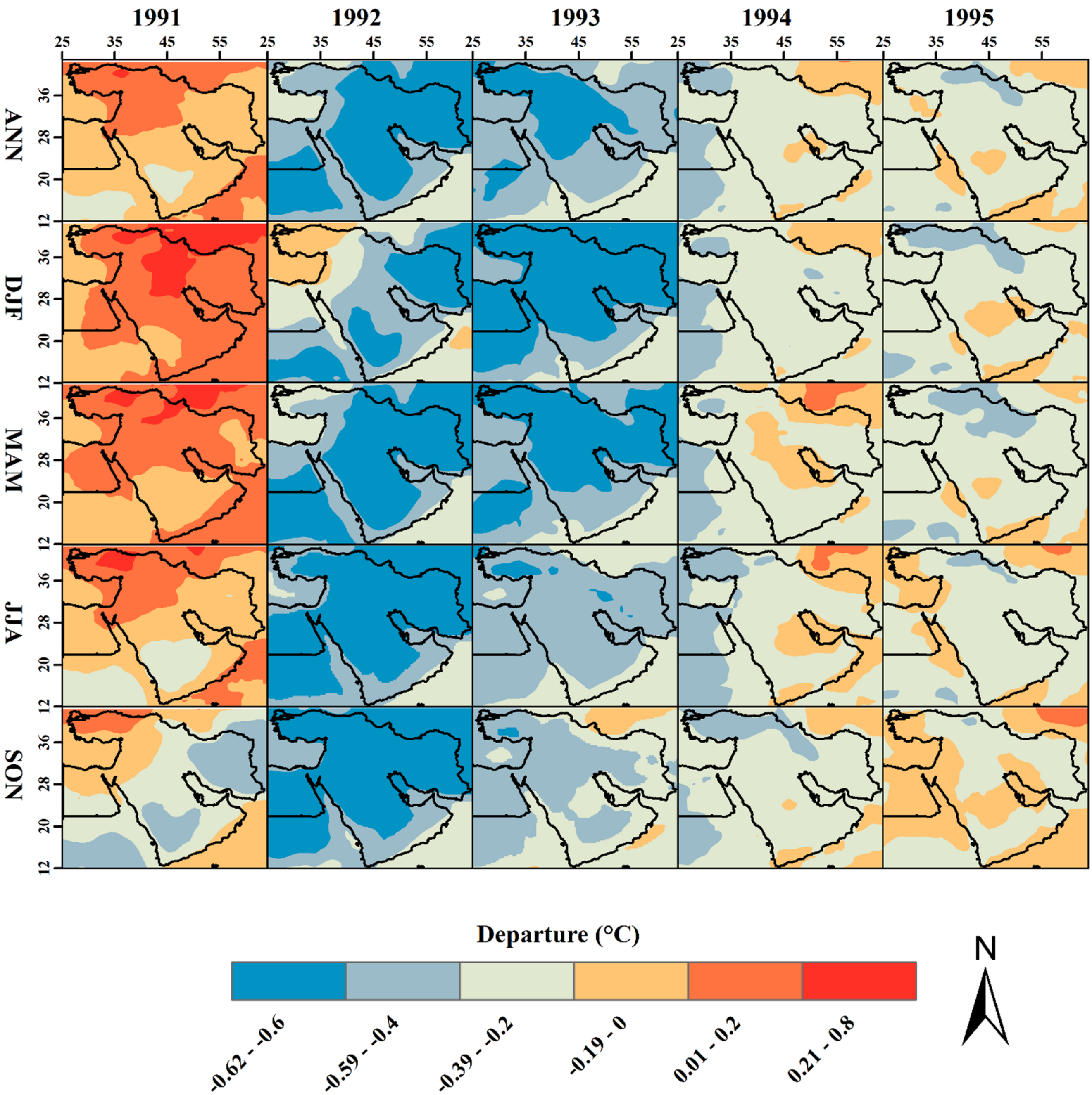

Fig. 10 Annual and seasonal temperature departures (1991–1995) relative to the five-year baseline before the Pinatubo eruption, where only cooling in the range of -0.20 to -0.62 °C is statistically significant

that cooling was highly variable depending on latitude. Specifically, tropical regions (0–30°N) recorded mean temperature departures of -0.3 °C, while high northern latitudes (60–90°N) experienced cooling of up to -1.0 °C.

Southern hemisphere (Krakatau)

Harvey and Grab (2022) used CMIP5 model outputs to estimate mean temperature departures of -0.3 °C and −0.37 °C for southern South America and southern Africa, respectively, for the first three post-eruption years. These values are not dissimilar to those for air temperatures recorded in Cape Town based on observational station data (Picas and Grab 2020), which showed a mean temperature departure of -0.3 °C for the first post-eruption year. However, the Cape Town data show significant inter-seasonal and inter-annual temperature variability following the Krakatau eruption. Specifically, post-eruption year 2 was warmer (+0.1 °C) than pre-eruption conditions, and post-eruption year 3 was substantially cooler again (-0.4 °C).

Middle East (Krakatau)

Our results for the Middle East, indicating a mean temperature departure of -0.51 °C, seem similar in amplitude to those of other global regions during the first 2–3 post-eruption years. However, these results differ from some patterns observed in the SH, particularly in post-eruption year 2. The renewed cooling (~ -0.2 °C) that affected 53.21% of the Middle East in 1887, noted in a variety of other global regions, is likely a consequence of the 1886 Tarawera eruption (Rampino and Self 1982; Picas and Grab 2020; Harvey and Grab 2021). This suggests that the Middle East was impacted by a so-called 'volcanic double' effect (Toohey et al. 2016) over the period 1883–1889, with prolonged cooling (particularly in the northernmost regions) possibly due to the combined climate impacts of Krakatau and Tarawera.

Agung 1963

Despite the smaller eruption of Agung in 1963, compared to Krakatau and Pinatubo, it likely induced a similar scale of global temperature reduction (~0.2 to 0.5 °C) during at least the first post-eruption year, based on observational station data (Self et al. 1981). However, a more recent study (Erlat and Türkeş 2019), based on observational data, suggested that winter cooling over Turkey (Middle East) was likely only −0.3 °C following the Agung eruption, approximately half of the cooling caused by the 1991 Pinatubo eruption. In Australia, a widespread and persistent temperature drop was recorded, with seasonal anomalies exceeding −0.4 °C across all seasons in the first post-eruption year, particularly in spring (−0.42 °C). Southeastern Australia showed the strongest and most coherent cooling patterns. In southern Africa, significant cooling was observed in the first year during winter (−0.39 °C) and autumn (−0.34 °C), with moderate anomalies extending into the second year in summer (−0.25 °C)) Harvey and Grab 2022(. In southern South America, the response was more delayed and scattered, with notable cooling during the winter of 1964 (−0.24 °C) and autumn of 1966 (−0.26 °C), suggesting a lagged and less uniform impact. In addition, studies have shown that although the global average forcing generated by the 1963 Agung eruption was weaker than that of Pinatubo (maximum value of about −2.5 W/m2), the effects were much stronger in the SH than in the NH (Harvey and Grab 2022).

Pinatubo 1991

The CMIP5 outputs for the SH suggest limited cooling (-0.23 °C) over southern South America during the first three post-eruption years, and that this cooling was restricted to only the first post-eruption year (-0.35 °C) over southern Africa (Harvey and Grab 2022). Our results for the Middle East indicate a much longer cool anomaly (~3 years) and more substantial cooling (-0.43 °C) than what has been reported for other parts of the world. The amplitude of cooling was not dissimilar to that of the larger magnitude Krakatau eruption, which is consistent with the earlier findings by Self et al. (1981). Our findings are consistent with studies conducted for the Middle East region (Dogar et al. 2017; Erlat and Türkeş 2019). For example, Dogar et al. (2017) found that winter cooling after the 1991 Pinatubo eruption far exceeded the mean hemispheric temperature anomaly almost 3 times in predominantly in North Africa and northern part of Arabian Peninsula. Erlat and Türkeş (2019) revealed that the 1991 Pinatubo eruption had the most remarkable temperature response over Turkey during the second winter, especially when compared to the Agung and El Chichón eruptions. The cooling magnitude of mean maximum temperature (mean minimum) was determined as −1.55 °C (−1.38 °C) in year+1 and −1.29 °C (−1.09 °C) in year+2, based on all seasons according to the 70 meteorological stations in Turkey. This long cool anomaly has not been supported in other studies and is likely an artifact of other climate dynamical factors not associated with volcanic forcing.

General trends (Pinatubo 1991)

Although the 1991 Pinatubo eruption reduced mean global air temperatures by 0.5–0.6 °C during 1992/3, the cooling effect was short-lived, and temperatures recovered almost immediately after 1993 (Eliseev and Mokhov 2008; Stoffel et al. 2015). More recent model outputs suggest that such levels of cooling are 'overrated' and that cooling likely only averaged 0.2 °C over 13 months (Boretti 2024). Cooling in the SH appears to have been moderate, averaging −0.23 °C in southern South America and −0.3 °C in southern Africa, according to CMIP5 model outputs (Hanvey and Grab, 2022).

Middle East (Pinatubo 1991)

Mean temperature departures in the Middle East were between −0.4 to -0.6 °C during 1992/3, which seems relatively strong compared to global and other regional patterns. Furthermore, our results indicate substantial cooling (-0.72 °C) during mid-summer of 1992 and a lengthy cool anomaly that lasted 10 years post-eruption. This prolonged cool anomaly has not been supported in other studies and is likely an artifact of other climate dynamical factors not associated with volcanic forcing.

To summarize, of the three major volcanic eruptions (Krakatau, Agung, and Pinatubo) we investigate for temperature responses in the Middle East, the strongest cooling anomalies were observed for the post-Krakatau period. This is unsurprising given the larger magnitude of that event compared to the other two eruptions. The response following Krakatau may also not have been as strongly masked by anthropogenic warming, as would have been the case for the latter two eruptions during the second half of the 20th century (Hopcroft et al. 2018). Recent climate model experiments suggest that the significant rise in ocean heat content and sea level (due to thermal expansion) observed throughout the 20th century was notably reduced by the 1883 eruption of Krakatau. The cooling effect induced by this volcanic event on the ocean's surface was transferred to deeper ocean layers, where it remained for several decades. In contrast, the temporary cooling of ocean heat content following the eruptions of El Chichón (1982) and Pinatubo (1991) was much more short-lived due to the rapidly changing, anthropogenically-driven increase in ocean temperatures during that period, making the cooling effect less sustained (Gleckler et al. 2006).

Comparing temperature patterns following the Krakatau-Agung-Pinatubo eruptions

Temperature responses following the three eruptions were spatially and temporally highly variable over the Middle East. Cooling gradually commenced from northern parts to southern regions during the first post-eruption year in the case of Krakatau. This was accompanied by strongest cooling during boreal spring. During the second post-eruption year, the strongest cooling occurred in winter, after which warming commenced from southern regions northwards. Southernmost regions (Yemen, United Arab Emirates, Oman) were thus least impacted by cooling, both in magnitude and duration. In contrast, northernmost regions had longest lasting cool anomalies. Although strong cooling was again observed over northern and central parts of the Middle East following the Agung eruption, such cooling did not progress much further southwards, as was the case with Krakatau. Consequently, southern and southwestern regions remained relatively unimpacted and indicate warm anomalies by mid-1965. The cooling pattern for Pinatubo begins during the Boreal autumn of 1991, extending as a 'band' from the southwestern to northeastern Middle East. This 'band' of cooling then gradually expands and intensifies across most of the Middle East during 1992, reaching its maximum extent during autumn/winter of 1992/3. Thereafter, the cool anomaly gradually dissipates but lasts longest over western parts of the Middle East. In contrast, eastern parts of the Middle East warm up most rapidly. To summarize, such diverse spatial patterns of cooling and warming following major volcanic eruptions, imply that multiple factors likely influence both the extent of cooling and spatio-temporal nature of cooling/warming over the Middel East, as is similarly the case for other global regions impacted by volcanic forcing (e.g. Picas and Grab 2020; Harvey and Grab 2021).

Although the three major volcanic eruptions examined in this study—Krakatau (1883), Agung (1963), and Pinatubo (1991)—differed in intensity, timing, and sulfate loading, the temperature response across the Middle East reveals a consistent regional pattern. In all three cases, a clear cooling signal emerged during the first post-eruption year, with the most pronounced temperature anomalies concentrated over northern, elevated, and inland parts of the region. In contrast, southern and coastal zones, particularly those adjacent to warm water bodies such as the Persian Gulf, Red Sea, and Gulf of Oman, experienced more subdued cooling effects. Despite variability in the magnitude and duration of cooling, the temporal extent of post-eruption anomalies ranged between approximately two to six years, suggesting that both eruption-specific characteristics (e.g., eruption latitude and SO_2 injection) and region-specific factors (e.g., topography, land-sea contrasts, and prevailing atmospheric dynamics) jointly shaped the regional response. Notably, even the moderate-magnitude Agung eruption produced substantial thermal anomalies, comparable in spatial pattern—though not duration—to those induced by Krakatau and Pinatubo. This convergence in regional responses indicates the inherent climatic sensitivity of the Middle East to stratospheric aerosol forcing. Moreover, in all three cases, thermal recovery was initiated in the southern and low-lying parts of the region and gradually expanded northward. These findings underscore the importance of integrating multi-model ensemble outputs, such as those from CMIP6, to isolate robust signals of volcanic influence and better understand the mechanisms governing spatial and temporal heterogeneity in post-eruption climatic behavior across complex regions like the Middle East.

Possible causes for post-eruption temperature patterns

We consider several possible factors that may contribute to the varied temperature responses across the Middle East. It is widely known that a variety of factors such as the timing, location, magnitude, and chemical composition of an eruption, along with other global- to regional-scale climate conditional factors (e.g. ENSO), will lead to diverse volcanically-forced temperature responses (Zambri et al. 2017; Alfaro-Sánchez et al. 2018; Dee et al. 2020). To this end, our focus is on possible regional factors that may account for disparate patterns of volcanically-induced cooling across the Middel East.

Although higher elevations generally experience more pronounced temperature fluctuations (Beniston 2006; Barry 2013; Pepin et al. 2022), it remains unclear whether volcanic eruptions have a more significant effect on temperature in these regions compared to adjoining lower elevations. The thinner atmosphere at higher elevations could potentially amplify this effect, though the specific mechanisms associated with such possible interactions still require detailed investigation (Robock 2000; Barry 2008; Timmreck 2012; Lelieveld et al. 2012). Notwithstanding such ongoing uncertainties, the occurrence of substantive elevated terrain (3000 to >5000 m asl), such as the Zagros Mountains, Alborz Mountains, and the highlands of Turkey (including the Taurus and Anti-Taurus Ranges), enhances the sensitivity of these areas to temperature fluctuations. In the extensive high elevation regions across the northern Middle East, the combined effects of volcanic aerosols and thinner atmosphere could potentially more strongly diminish incoming solar radiation and amplify cooling. Conversely, the southern Middle East, characterized by warm water bodies such as the Persian Gulf, the Sea of Oman, and the Red Sea, encounters moderating cooling effects (Alosairi et al. 2020). These water bodies, with their high heat capacity, gradually release stored heat, thereby retarding temperature reductions over adjacent areas. However, such thermal moderation predominantly only affects the lower atmospheric layers.

Northernmost parts of the Middle East are located at relatively high latitude (~40°N) where baseline solar radiation levels are comparatively lower than southernmost (~10°N) regions. Consequently, any additional reduction in solar radiation caused by volcanic aerosols is likely to induce more substantial cooling from southern to northern parts, as is observed. A further important factor to consider is atmospheric circulation. Volcanic sulfate aerosols, which are injected into the stratosphere during eruptions, are often transported towards higher latitudes by prevailing winds and large-scale atmospheric circulation systems. This process leads to a higher concentration of aerosols over high latitude regions, thereby intensifying the cooling effect in those areas, compared to lower latitude regions (Oman et al. 2005; Schneider et al. 2009). Aerosols from tropical volcanic eruptions (e.g. Pinatubo) spread over the entire globe, whereas high-latitude eruptions typically have aerosols which remain in the hemisphere in which they were injected.

In our study, however, all three eruptions may be considered as tropical in location. Nonetheless, subtle differences of almost 20° latitude between the Pinatubo (15°N) and Agung (8°S) eruptions might be sufficient to impose the notable differences in temperature response patterns observed across the Middle East, not least because Pinatubo had a stronger sulfate aerosol loading into the NH, and the converse happened with Agung (Self et al. 1981; Sigl et al. 2022). It is important to note that the temperature responses discussed here are derived from model simulations, not observational data. In the models, the eruptions are treated as occurring at the same latitude, so the observed differences in temperature response across regions are not directly linked to latitude but rather to the different characteristics of the eruptions, such as the amount of aerosol released and its impact on the atmosphere.

A further factor contributing to the cooling trend observed after volcanic eruptions in the Mediterranean and Middle East is the positive phases of the North Atlantic Oscillation (NAO) (Dogar et al. 2017; Van Dijk et al. 2022). The transition of the NAO to a positive phase after a strong volcanic eruption at low latitudes is explained by the warming of the lower stratosphere in the tropics, associated with the absorption of long-wave radiation by volcanic aerosols (DallaSanta et al. 2019; Weierbach et al. 2023). Warming in the lower stratosphere increases the equator-pole stratospheric temperature gradients, which in turn causes an anomalously strong polar vortex, causing the NAO to transition to a positive phase (Handler 1989; Baldwin and Dunkerton 1999; Ambaum and Hoskins 2002). Such processes are likely to more strongly impact western parts of the Middel East and hence, in part, might account for prolonged cooling in such regions following major eruptions such as was the case with Pinatubo.

Analyzing the impacts of volcanic-induced cooling in the Middle East

The recorded post-eruption temperature decreases in the Middle East, ranging from 0.2 °C to 0.8 °C, may appear minor in absolute terms. However, within the context of the region's hot and arid climate, such anomalies can have substantial implications. The Middle East is characterized by arid to hyper-arid climatic zones, where average summer temperatures often exceed 35 °C, and in some areas, even surpass 45 °C. According to reports by the World Meteorological Organization and the Intergovernmental Panel on Climate Change (Masson-Delmotte et al. 2021; IPCC, 2021), even small temperature variations (e.g. 0.2 °C) can influence the regional energy balance, evapotranspiration rates, water demand, and agricultural productivity. Furthermore, the Food and Agriculture Organization of the

United Nations (FAO) reports that short-term cooling can disrupt the timing of growing seasons in semi-arid regions, potentially triggering severe fluctuations in food production (Bélanger and Pilling 2019).

From a climatological standpoint, the significance of such anomalies becomes particularly evident when considering their influence on broader climate variability and extreme weather events. The IPCC (2021) indicates that sudden cooling or warming, even by fractions of a degree, can alter atmospheric circulation patterns, displace jet streams, and disrupt the spatial and temporal distribution of precipitation. In the Middle East, where chronic water stress, erratic rainfall, and increasing pressure on natural resources prevail, volcanic-induced cooling may temporarily alleviate regional heat stress but could simultaneously intensify the volatility of precipitation systems and increase the frequency of abrupt droughts. Therefore, the implications of volcanic activity on temperature must not be evaluated solely in terms of the magnitude of cooling, but rather through the lens of regional climate dynamics and the vulnerability of human and environmental systems.

Limitations and future perspectives

This study is subject to several limitations that should be addressed in future research. One notable limitation lies in the reliance on climate model outputs and historical reconstructions, which may carry inherent uncertainties in simulating volcanic forcings and the complex interactions within the climate system. Additionally, the interactions among different atmospheric layers, which can significantly influence climate responses at varying temporal and spatial scales, were not fully considered in this study. Given the natural spatial and temporal limitations of CMIP6 simulations, future studies should focus on improving model resolution, particularly at smaller regional scales, and further investigate the role of teleconnection patterns and upper-tropospheric circulation dynamics. Moreover, integrating new observational and empirical data could help reduce the uncertainties associated with model-based results and provide a more comprehensive understanding of regional climate responses to volcanic activity.

Conclusion

This study examined the response of air temperature across the Middle East to major tropical volcanic eruptions over the past 150 years, using outputs from CMIP6 climate models. The simulations consistently demonstrate that large tropical eruptions induce discernible temperature anomalies in the region. While an overall cooling trend is evident following eruptions, the magnitude and spatial expression of this cooling vary considerably, influenced by internal climate variability, seasonal dynamics, and prevailing background conditions at the time of each event.

Our analysis reveals a marked decline in air temperatures over the Middle East following the three prominent tropical eruptions: Krakatoa (1883), Agung (1963), and Pinatubo (1991). Specifically, negative temperature anomalies were observed during the 75-month period after the Krakatau eruption, the 43-month period following the Agung eruption, and the estimated 52-month period following the Pinatubo event (from August 1991 to March 1996, subject to further verification), based on deviations from a five-year pre-eruption climatological baseline. Although the magnitude and persistence of cooling are modulated by factors such as the presence of subsequent volcanic activity and variability in teleconnection phases, the Volcanic Explosivity Index (VEI) emerges as a key determinant in the regional climate response. The Krakatau (VEI 6.4) and Pinatubo (VEI 6.1) eruptions, in particular, produced the strongest radiative forcing and the most pronounced temperature responses.

The peak regional cooling in response to the three eruptions occurred approximately 10 to 14 months after each event. Maximum mean temperature anomalies were recorded as −0.74 °C in May–June 1884 (post-Krakatau), −0.76 °C in July 1992 (post-Pinatubo), and −0.59 °C in May 1964 (post-Agung), reflecting the significant thermal impacts of these events on regional climate.

The spatial distribution of post-eruption cooling exhibited notable heterogeneity across the Middle East. This variability appears to be modulated by elevation, latitude, and large-scale atmospheric circulation patterns, in addition to eruption magnitude. The most substantial cooling effects were observed at higher elevations, and northern sub-regions exhibited greater sensitivity to volcanic forcing compared to southern areas. Furthermore, the extended and more intense cooling observed over the western Middle East, particularly following the 1991 Pinatubo eruption, may be partially attributed to the influence of the North Atlantic Oscillation (NAO).

The seasonality of the cooling response was also evident. The most pronounced and spatially extensive cooling occurred during spring and winter in the two years following each eruption. In spring, the cooling is likely linked to the reduced transmission of incoming shortwave radiation caused by volcanic aerosols, despite the seasonal increase in solar insolation. During winter, the NAO frequently shifts into a positive phase after major eruptions, amplifying negative temperature anomalies across the region.

The coherent post-eruption signals associated with the three tropical eruptions examined in this study suggest that seasonal air temperature anomalies over the Middle East following large volcanic events can be anticipated with a reasonable degree of confidence. Nonetheless, further high-resolution investigations are warranted to better understand the role of teleconnection patterns and upper-tropospheric circulation dynamics in modulating these climate responses.

Acknowledgements The authors' work was partially supported by the Golestan University, Golestan Province, Iran, under grant No. 1695. We thank Golestan University for their support in the project. We thank the CMIP6 initiative and all climate modeling groups for contributing to CMIP6 and making their model outputs available.

Author contributions "Conceptualization, A.A.G., and G.R.R.; methodology, A.A.G., and G.R.R.; software, A.A.G., and G.R.R.; validation, A.A.G., and S.W.G.; formal analysis, G.R.R., investigation, G.R.R., and A.A.G.; data curation, A.A.G., and G.R.,G.; writing—original draft preparation, G. R. R.; writing—review and editing, S.W.G., M.T., and E.E.; visualization, A.A.G., and G.R.R.; supervision, A.A.G., and S.W.G.; All authors have read and agreed to the published version of the manuscript."

Funding This work was partially supported by Golestan University, Golestan Province, Iran, under grant number 1695.

Data availability No datasets were generated or analysed during the current study.

Declarations

Ethics approval and consent to participate Not applicable, as this study does not involve human or animal subjects.

Consent for publication Not applicable, as this study does not include individual data, images, or videos.

Competing interests The authors declare no competing interests.

References

Alfaro-Sánchez R, Nguyen H, Klesse S, Hudson A, Belmecheri S, Köse N, Trouet V (2018) Climatic and volcanic forcing of tropical belt Northern boundary over the past 800 years. Nat Geosci 11(12):933–938

Alosairi Y, Alsulaiman N, Rashed A, Al-Houti D (2020) World record extreme sea surface temperatures in the Northwestern arabian/persian Gulf verified by in situ measurements. Mar Pollut Bull 161:111766

Ambaum MH, Hoskins BJ (2002) The NAO troposphere–stratosphere connection. J Clim 15(14):1969–1978

Baldwin MP, Dunkerton TJ (1999) Propagation of the Arctic Oscillation from the stratosphere to the troposphere. J Geophys Research: Atmos 104(D24):30937–30946

Barry RG (2008) Mountain weather and climate. – Cambridge University Press, New York

Barry RG (2013) Mountain weather and climate. Routledge

Bélanger J, Pilling D (2019) The state of the world's biodiversity for food and agriculture. FAO

Beniston M (2006) Mountain weather and climate: a general overview and a focus on Climatic change in the alps. Hydrobiologia 562:3–16

Bilbao R, Ortega P, Swingedouw D, Hermanson L, Athanasiadis P, Eade R, Devilliers M, Doblas-Reyes F, Dunstone N, Ho A-C, Merryfield W, Mignot J, Nicolì D, Samsó M, Sospedra-Alfonso R, Wu X, Yeager S (2024) Impact of volcanic eruptions on CMIP6 decadal predictions: a multi-model analysis. Earth Sys Dyn 15:501–525. https://doi.org/10.5194/esd-15-501-2024

Boretti A (2024) Reassessing the cooling that followed the 1991 volcanic eruption of Mt. Pinatubo J Atmospheric Solar Terr Phys 256:106187

Briffa KR, Jones PD, Schweingruber FH, Osborn TJ (1998) Influence of volcanic eruptions on Northern hemisphere summer temperature over the past 600 years. Nature 393(6684):450–455

Climatic Research Unit. (n.d.). North Atlantic Oscillation (NAO) data. University of East Anglia. Available (2024) Retrieved from https://crudata.uea.ac.uk/cru/data/nao/values.htm

Collins WD, Rasch PJ, Boville BA, Hack JJ, McCaa JR, Williamson DL, Zhang M (2006) The formulation and atmospheric simulation of the community atmosphere model version 3 (CAM3). J Clim 19(11):2144–2161

Colose CM, LeGrande AN, Vuille M (2015) The influence of tropical volcanic eruptions on the climate of South America during the last millennium. Clim Past 11(4):3375–3424

Coupe J, Robock A (2021) The influence of stratospheric soot and sulfate aerosols on the northern hemisphere wintertime atmospheric circulation. J Geophys Res Atmos 126(11):e2020JD034513

DallaSanta K, Gerber EP, Toohey M (2019) The circulation response to volcanic eruptions: the key roles of stratospheric warming and eddy interactions. J Clim 32(4):1101–1120

Dee SG, Cobb KM, Emile-Geay J, Ault TR, Edwards RL, Cheng H, Charles CD (2020) No consistent ENSO response to volcanic forcing over the last millennium. Science 367(6485):1477–1481

Dogar MM, Stenchikov G, Osipov S, Wyman B, Zhao M (2017) Sensitivity of the regional climate in the Middle East and North Africa to volcanic perturbations. J Geophys Research: Atmos 122(15):7922–7948

Dogar MMA, Fujiwara M, Ohba M, Almazroui M (2025) Investigating post-eruption amplified winter cooling in the Middle East and North Africa—unraveling ENSO and NAO dynamics. Environmental Research Communications

Eliseev AV, Mokhov II (2008) Influence of volcanic activity on climate change in the past several centuries: assessments with a climate model of intermediate complexity. Izv Atmospheric Ocean Phys 44:671–683

Erlat E, Türkeş M (2019) Temperature responses of turkey's climate to the tropical volcanic eruptions over second half of the twentieth century. Theoret Appl Climatol 137:2369–2379

Eyring V, Bony S, Meehl GA, Senior CA, Stevens B, Stouffer RJ, Taylor KE (2016) Overview of the coupled model intercomparison project phase 6 (CMIP6) experimental design and organization. Geosci Model Dev 9(5):1937–1958

Fischer EM, Luterbacher J, Zorita E, Tett SFB, Casty C, Wanner H (2007) European climate response to tropical volcanic eruptions over the last half millennium. Geophys Res Lett 34(5)

Fujiwara M, Hibino T, Mehta SK, Gray L, Mitchell D, Anstey J (2015) Global temperature response to the major volcanic eruptions in multiple reanalysis data sets. Atmos Chem Phys 15(23):13507–13518

Gerber EP, Pausata FS, Ball WT, Bauer SE, Dhomse SS, LeGrande AN, Mann GW (2016) The Model Intercomparison Project on the climatic response to Volcanic forcing (VolMIP): experimental design and forcing input data for CMIP6. Geoscientific Model Development, 9(8), p.2701

Gleckler PJ, AchutaRao K, Gregory JM, Santer BD, Taylor KE, Wigley TML (2006) Krakatoa lives: the effect of volcanic eruptions on ocean heat content and thermal expansion. Geophys Res Lett 33(17)
Handler P (1989) The effect of volcanic aerosols on global climate. J Volcanol Geoth Res 37(3–4):233–249
Harvey PJ, Grab SW (2021) Southern African temperature responses to major volcanic eruptions since 1883: simulated by CMIP5 models. Int J Climatol 41(11):5386–5405
Harvey PJ, Grab SW (2022) Australian sub-regional temperature responses to volcanic forcing: A critical analysis using CMIP5 models. Int J Climatol 42(12):6109–6125
Harvey PJ, Grab SW, Malherbe J (2020) Major volcanic eruptions and their impacts on Southern hemisphere temperatures during the late 19th and 20th centuries, as simulated by CMIP5 models. Geophys Res Lett 47(14), e2020GL087792
Haurwitz MW, Brier GW (1981) A critique of the superposed epoch analysis method: its application to solar-weather relations. Mon Weather Rev 109(10):2074–2079
Hopcroft PO, Kandlbauer J, Valdes PJ, Sparks RSJ (2018) Reduced cooling following future volcanic eruptions. Clim Dyn 51(4):1449–1463
Hua W, Dai A, Zhou L, Qin M, Chen H (2019) An externally forced decadal rainfall Seesaw pattern over the Sahel and Southeast Amazon. Geophys Res Lett 46:923–932
IPCC (2021) Climate change 2021: the physical science basis. Contribution of working group I to the sixth assessment report of the intergovernmental panel on climate change. Cambridge University Press
Issar A (2003) Water, environment and history in the Middle East. Springer
Issar AS, Zohar M (2007) Climate change: environment and history of the near East. Springer
Lelieveld J, Hadjinicolaou P, Kostopoulou E, Chenoweth J, Maayar E, Giannakopoulos M, C.,&, Xoplaki E (2012) Climate change and impacts in the Eastern mediterranean and the Middle East. Clim Change 114:667–687
Li J, Miao C, Wei W, Zhang G, Hua L, Chen Y, Wang X (2021) Evaluation of CMIP6 global climate models for simulating land surface energy and water fluxes during 1979–2014. J Adv Model Earth Syst 13(6), e2021MS002515
Man W, Zhou T, Jungclaus JH (2014) Effects of large volcanic eruptions on global summer climate and East Asian monsoon changes during the last millennium: analysis of MPI-ESM simulations. J Clim 27(19):7394–7409
Masson-Delmotte V, Zhai P, Pirani A, Connors SL, Péan C, Berger S, Zhou B (2021) Climate change 2021: the physical science basis. Contribution Working Group I Sixth Assess Rep Intergovernmental Panel Clim Change 2(1):2391
McBride LA, Hope AP, Canty TP, Bennett BF, Tribett WR, Salawitch RJ (2021) Comparison of CMIP6 historical climate simulations and future projected warming to an empirical model of global climate. Earth Sys Dyn 12(2):545–579
Meehl GA, Teng H, Arblaster JM (2014) Climate model simulations of the observed early-2000s hiatus of global warming. Nat Clim Change 4(10):898–902
Myhre G, Shindell D, Bréon FM, Collins W, Fuglestvedt J, Huang J, Koch D, Lamarque JF, Lee D, Mendoza B, Nakajima T, Robock A, Stephens G, Takemura T, Zhang H (2013) Anthropogenic and natural radiative forcing. In: Stocker TF, Qin D, Plattner GK, Tignor M, Allen SK, Boschung J, Nauels A, Xia Y, Bex V, Midgley PM (eds) Climate change 2013: the physical science basis. Contribution of working group I to the fifth assessment report of the intergovernmental panel on climate change. Cambridge University Press, pp 659–740. https://doi.org/10.1017/CBO9781107415324.018
Neira M, Erguler K, Ahmady-Birgani H, Al-Hmoud ND, Fears R, Gogos C, Hobbhahn N, Koliou M, Kostrikis LG, Lelieveld J, Majeed A (2023) Climate change and human health in the Eastern mediterranean and Middle east: literature review, research priorities and policy suggestions. Environ Res 216:p114537
Neukom R, Gergis J, Karoly DJ, Wanner H, Curran M, Elbert J, González-Rouco F, Linsley BK, Moy AD, Mundo I, Raible CC (2014) Inter-hemispheric temperature variability over the past millennium. Nat Clim Change 4(5):362–367
Newhall CG, Self S (1982) The volcanic explosivity index (VEI) an estimate of explosive magnitude for historical volcanism. J Phys Res 87(C2):1231–1238
Nijsse FJ, Cox PM, Williamson MS (2020) Emergent constraints on transient climate response (TCR) and equilibrium climate sensitivity (ECS) from historical warming in CMIP5 and CMIP6 models. Earth Sys Dyn 11(3):737–750
O'Neill BC, Tebaldi C, Van Vuuren DP, Eyring V, Friedlingstein P, Hurtt G, Knutti R, Kriegler E, Lamarque JF, Lowe J, Meehl GA (2016) The scenario model intercomparison project (ScenarioMIP) for CMIP6. Geosci Model Dev 9(9):3461–3482
Oman L, Robock A, Stenchikov G, Schmidt GA, Ruedy R (2005) Climatic response to high-latitude volcanic eruptions. J Phys Res 110:D13103
Paik S, Min SK, Son SW, Lim EP, McGregor S, An SI, Yeh SW (2023) Impact of volcanic eruptions on extratropical atmospheric circulations: review, revisit and future directions. Environ Res Lett 18(6):063003
Pepin NC, Arnone E, Gobiet A, Haslinger K, Kotlarski S, Notarnicola C, Adler C (2022) Climate changes and their elevational patterns in the mountains of the world. Rev Geophys 60(1), e2020RG000730
Picas J, Grab SW (2020) Potential impacts of major nineteenth century volcanic eruptions on temperature over cape town, South africa: 1834–1899. Clim Change 159:523–544
Raible CC, Brönnimann S, Auchmann R, Brohan P, Frölicher TL, Graf HF, Wegmann M (2016) Tambora 1815 as a test case for high impact volcanic eruptions: Earth system effects. Wiley Interdisciplinary Reviews: Clim Change 7(4):569–589
Rampino MR, Self S (1982) Historic eruptions of Tambora (1815), Krakatau (1883), and Agung (1963), their stratospheric aerosols, and Climatic impact. Quatern Res 18(2):127–143
Rao MP, Cook BI, Cook ER, D'Arrigo RD, Krusic PJ, Anchukaitis KJ, LeGrande AN, Buckley BM, Davi NK, Leland C, Griffin KL (2017) European and mediterranean hydroclimate responses to tropical volcanic forcing over the last millennium. Geophys Res Lett 44:5104–5112
Rao MP, Cook ER, Cook BI, Anchukaitis KJ, D'Arrigo RD, Krusic PJ, LeGrande AN (2019) A double bootstrap approach to superposed epoch analysis to evaluate response uncertainty. Dendrochronologia 55:119–124
Rieger LA, Cole JN, Fyfe JC, Po-Chedley S, Cameron-Smith PJ, Durack PJ, Tang Q (2020) Quantifying CanESM5 and EAMv1 sensitivities to volcanic forcing for the CMIP6 historical experiment. Geoscientific Model Dev Discuss 2020:1–17
Robock A (2000) Volcanic eruptions and climate. Rev Geophys 38(2):191–219
Rong X, Li J, Chen H, Su J, Hua L, Zhang Z, Xin Y (2021) The CMIP6 historical simulation datasets produced by the climate system model CAMS-CSM. Adv Atmos Sci 38:285–295
Schaller N, Griesser T, Fischer A, Stickler A, Onnimann S (2009) Climate effects of the 1883 krakatoa eruption: historical and present perspectives. Vjschr Natf Ges Zürich 154:31–40
Schmidt A, Black BA (2022) Reckoning with the Rocky relationship between eruption size and climate response: toward a volcano-climate index. Annu Rev Earth Planet Sci 50(1):627–661

Schneider DP, Ammann CM, Otto-Bliesner BL, Kaufman DS (2009) Climate response to large, high-latitude and low-latitude volcanic eruptions in the community climate system model. J Phys Res 114:D15101

Self S (2006) The effects and consequences of very large explosive volcanic eruptions. Philosophical Trans Royal Soc A: Math Phys Eng Sci 364(1845):2073–2097

Self S, Rampino MR, Barbera JJ (1981) The possible effects of large 19th and 20th century volcanic eruptions on zonal and hemispheric surface temperatures. J Volcanol Geoth Res 11(1):41–60

Shindell DT, Schmidt GA, Miller RL, Mann ME (2004) Volcanic and solar forcing of climate change during the preindustrial era. J Clim 16(24):4094–4107

Sigl M, Winstrup M, McConnell JR, Welten KC, Plunkett G, Ludlow F, Woodruff TE (2015) Timing and climate forcing of volcanic eruptions for the past 2,500 years. Nature 523(7562):543–549

Sigl M, Toohey M, McConnell JR, Cole-Dai J, Severi M (2022) Volcanic stratospheric sulfur injections and aerosol optical depth during the holocene (past 11 500 years) from a bipolar ice-core array. Earth Syst Sci Data 14(7):3167–3196

Smith CJ, Kramer RJ, Myhre G, Alterskjær K, Collins W, Sima A, Forster PM (2020) Effective radiative forcing and adjustments in CMIP6 models. Atmos Chem Phys 20(16):9591–9618

Stoffel M, Khodri M, Corona C, Guillet S, Poulain V, Bekki S, Masson-Delmotte V (2015) Estimates of volcanic-induced cooling in the Northern hemisphere over the past 1,500 years. Nat Geosci 8(10):784–788

Suhadha AG, Harintaka H (2024) Multidimensional displacement analysis of Semeru volcano, Indonesia following December 2021 eruption from Multitrack InSAR observation. Earth Sci Inf 17(2):1539–1552

Tejedor E, Steiger NJ, Smerdon JE, Serrano-Notivoli R, Vuille M (2021) Global hydroclimatic response to tropical volcanic eruptions over the last millennium. Proceedings of the National Academy of Sciences 118(12), e2019145118

Thompson DW, Wallace JM, Jones PD, Kennedy JJ (2009) Identifying signatures of natural climate variability in time series of global-mean surface temperature: methodology and insights. J Clim 22(22):6120–6141

Timmreck C (2012) Modeling the Climatic effects of large explosive volcanic eruptions. WIREs Clim Change 3(6):545–564

Timmreck C (2018) Climatic effects of large volcanic eruptions. Habilitation Thesis. Hamburg: Universität Hamburg

Toohey M, Krüger K, Sigl M, Stordal F, Svensen H (2016) Climatic and societal impacts of a volcanic double event at the dawn of the Middle ages. Clim Change 136:401–412

Toohey M, Krüger K, Schmidt H, Timmreck C, Sigl M, Stoffel M, Wilson R (2019) Disproportionately strong climate forcing from extratropical explosive volcanic eruptions. Nat Geosci 12(2):100–107

Tramblay Y, Koutroulis A, Samaniego L, Vicente-Serrano SM, Volaire F, Boone A, Polcher J (2020) Challenges for drought assessment in the mediterranean region under future climate scenarios. Earth Sci Rev 210:103348

Türkeş M (2017) Recent spatiotemporal variations of synoptic meteorological sand and dust storm events observed over the Middle East and surrounding regions. In Proceedings of the 5th International Workshop on Sand and Dust Storms (SDS): Dust Sources and their Impacts in the Middle East (pp. 23–25)

Türkeş M (2020) Climate and drought in Türkiye. In: Harmancioglu NB, Altinbilek D (eds) Water resources of türkiye, world water resources, vol 2. Springer, Cham, pp 85–125

Türkeş M (2022) Climatology and meteorology. Updated and expanded second edition. Kriter, İstanbul. (In Turkish)

Türkeş M, Turp MT, An N, Ozturk T, Kurnaz ML (2020) Impacts of climate change on precipitation climatology and variability in Turkey. In: Harmancioglu N, Altinbilek D (eds) Water resources of turkey. World water resources, vol 2. Springer, Cham, pp 467–491

Uslular G, Kıyıkçı F, Karaarslan E, Kuşcu GG (2022) Application of machine-learning algorithms for tephrochronology: a case study of Plio-Quaternary volcanic fields in the South Aegean active volcanic Arc. Earth Sci Inf 15(2):1167–1182

Van Dijk E, Jungclaus J, Lorenz S, Timmreck C, Krüger K (2022) Was there a volcanic-induced long-lasting cooling over the Northern hemisphere in the mid-6th–7th century? Clim Past 18(7):1601–1623

Weierbach H, LeGrande AN, Tsigaridis K (2023) The impact of ENSO and NAO initial conditions and anomalies on the modeled response to Pinatubo-sized volcanic forcing. Atmos Chem Phys 23(24):15491–15505

Wen-Min M, Meng Z (2019) Short commentary on CMIP6 Model Intercomparison Project on the climatic response to Volcanic forcing (VolMIP). Advances in Climate Change Research 15(5), 526

Wilmes SB, Raible CC, Stocker TF (2012) Climate variability of the mid- and high-latitudes of the Southern hemisphere in ensemble simulations from 1500 to 2000 AD. Clim Past 8(1):373–390

Zambri B, LeGrande AN, Robock A, Slawinska J (2017) Northern hemisphere winter warming and summer monsoon reduction after volcanic eruptions over the last millennium. J Geophys Research: Atmos 122:7971–7989

Zanchettin D, Timmreck C, Khodri M, Robock A, Hegerl G, Schmidt A, Toohey M, Pausata FS, Black B, Bothe O, English JM (2015) Application for a model intercomparison project on the Climatic response to volcanic forcing (VolMIP) as CMIP6-Endorsed MIP

Zelinka MD, Myers TA, McCoy DT, Po-Chedley S, Caldwell PM, Ceppi P, Taylor KE (2020) Causes of higher climate sensitivity in CMIP6 models. Geophys Res Lett 47(1), e2019GL085782

Zhu X, Ji Z, Liu F, Dong W, Gao C (2024) Extreme Tibetan plateau cooling caused by tropical volcanism. Clim Atmospheric Sci 7(1):122

Zielinski GA (2000) Use of paleo-records in determining variability within the volcanism–climate system. Q Sci Rev 19(1–5):417–438

Zittis G, Almazroui M, Alpert P, Ciais P, Cramer W, Dahdal Y, Fnais M, Francis D, Hadjinicolaou P, Howari F, Jrrar A (2022) Climate change and weather extremes in the Eastern mediterranean and Middle East. Rev Geophys 60(3):e2021RG000762